The Pinto shear zone; a Laramide synconvergent extensional shear zone in the Mojave Desert region of the southwestern United States

Michael L. Wells[a,*], Mengesha A. Beyene[a], Terry L. Spell[a], Joseph L. Kula[a], David M. Miller[b], Kathleen A. Zanetti[a]

[a]Department of Geoscience, University of Nevada Las Vegas, Las Vegas, NV 89154, USA
[b]U.S. Geological Survey, MS-973, 345 Middlefield Road, Menlo Park, CA 94025, USA

Abstract

The Pinto shear zone is one of several Late Cretaceous shear zones within the eastern fringe of the Mesozoic magmatic arc of the southwest Cordilleran orogen that developed synchronous with continued plate convergence and backarc shortening. We demonstrate an extensional origin for the shear zone by describing the shear-zone geometry and kinematics, hanging wall deformation style, progressive changes in deformation temperature, and differences in hanging wall and footwall thermal histories. Deformation is constrained between ∼74 and 68 Ma by $^{40}Ar/^{39}Ar$ thermochronology of the exhumed footwall, including multi-diffusion domain modeling of K-feldspar. We discount the interpretations, applied in other areas of the Mojave Desert region, that widespread Late Cretaceous cooling results from refrigeration due to subduction of a shallowly dipping Laramide slab or to erosional denudation, and suggest alternatively that post-intrusion cooling and exhumation by extensional structures are recorded. Widespread crustal melting and magmatism followed by extension and cooling in the Late Cretaceous are most consistent with production of a low-viscosity lower crust during anatexis and/or delamination of mantle lithosphere at the onset of Laramide shallow subduction.
© 2005 Elsevier Ltd. All rights reserved.

Keywords: Laramide tectonics; Synconvergent extension; Delamination; Mojave Desert

1. Introduction

The Mesozoic to early Cenozoic Sevier–Laramide orogens of the western US—segments of the larger Cordilleran orogen (Burchfiel et al., 1992)—are classic examples of backarc belts of crustal shortening, considered to be ancient and more deeply exhumed analogues to the modern Andean orogen (Burchfiel and Davis, 1976; Jordan et al., 1983; Isacks, 1988). Post-orogenic Cenozoic extension of the hinterland of the Sevier–Laramide orogen is well-recognized (Wernicke, 1992 and references therein) whereas older, synorogenic Cretaceous extension is more cryptic. Cretaceous extension has been documented in scattered mountain ranges of the Great Basin (Wells et al., 1990, 1998; Camilleri and Chamberlain, 1997) and Mojave

Desert regions (Carl et al., 1991; Applegate et al., 1992; Beyene et al., 2000; Wells et al., 2002) and was possibly an orogen-scale event (Hodges and Walker, 1992) (Fig. 1). Late Cretaceous extension was synchronous with continued convergence between the Farallon/Kula plates and western North America (Engebretson et al., 1985), continued shortening in the fold–thrust belt north of southern Utah (Decelles et al., 1995; Yonkee et al., 1997) and early shortening in the Laramide foreland province (e.g., Dickinson et al., 1988) (Fig. 1). Although prior crustal thickening during Sevier orogenesis undoubtedly played an important role in providing requisite lateral contrasts in crustal thickness to gravitationally drive Cretaceous extension, it remains unclear what changes in the dynamics of the orogen took place to trigger synconvergent extension. A change is required, otherwise compressional forces sufficient to initially thicken the crust to form an orogenic plateau would continue to support the plateau against gravitationally induced extension (Molnar and Lyon-Caen, 1988). To better understand the mechanisms triggering

---

* Corresponding author. Tel.: +1 7028953262; fax: +1 7028954064
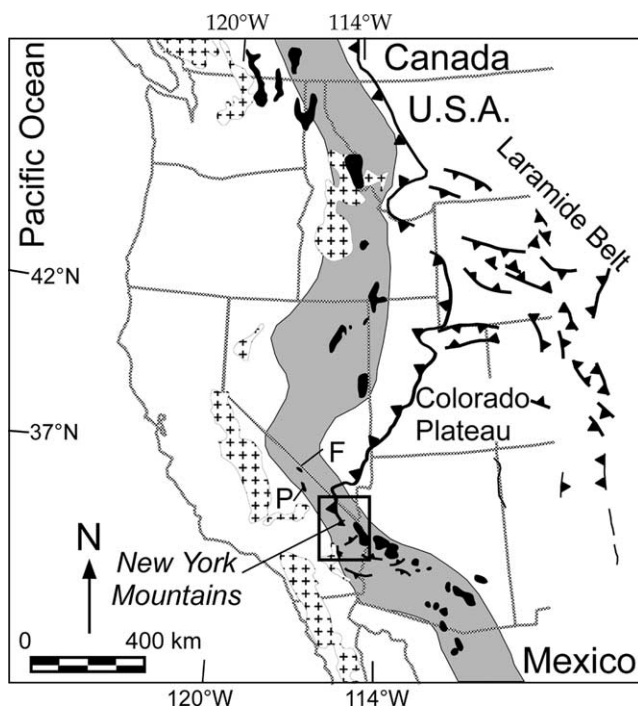E-mail address: mlwells@unlv.nevada.edu (M.L. Wells).

Fig. 1. Simplified tectonic map of the western Cordillera showing selected Cretaceous to early Tertiary features and location of study area. Belt of muscovite granites (grey fill; Miller and Bradfish, 1980) largely coincides with the belt of metamorphic core complexes (black fill) and inferred axis of maximum crustal thickening in the Cordilleran orogen. The leading edge of Cordilleran fold–thrust belt (bold lines with teeth) converges with the magmatic arc (cross pattern), towards the south in southeastern California. Box shows location of the study area (Fig. 2) in the eastern Mojave Desert. F, Funeral Mountains; P, Panamint Range.

Cretaceous extension in the southwestern Cordillera, it is important to establish whether the onset of extension was regionally synchronous, diachronous, or localized at any one time, and also whether there is a consistent relationship between the onset of extension and magmatism. Resolving these issues requires better age constraints on the inception and duration of extension, clear distinctions between extensional and contractional origins for structures, and additional geochronological studies of Cretaceous plutons.

The Cordillera of the southwest US is particularly well suited to establish better age constraints for Mesozoic deformation, and Cretaceous extension in particular, because the eastern fringe of the Mesozoic magmatic arc interacts with both contractional and extensional structures. For example, in the Old Woman Mountains area, thermochronometry and geobarometry of Cretaceous plutons shows rapid cooling from 73 to 68 Ma due to exhumation by syn- to post-magmatic extensional shear zones following thrust burial to mid-crustal depths (Carl et al., 1991; Foster et al., 1992; McKaffrey et al., 1999) (Fig. 2). Structural unroofing of metamorphic rocks in the Funeral Mountains of the Death Valley region (Fig. 1) occurred during intrusion of Late Cretaceous dikes and sills at 72 Ma (Hodges and Walker, 1990; Applegate et al., 1992;

Applegate and Hodges, 1995). K–Ar and ^{40}Ar/^{39}Ar cooling ages in other areas of the Mojave desert (Evernden and Kistler, 1970; Armstrong and Suppe, 1973; Kistler and Peterman, 1978; Miller and Morton, 1980; Jacobson, 1990; Foster et al., 1990) and southern Sierra (Wood and Saleeby, 1997) suggest the possibility of regional extension at 75–68 Ma. However, alternative mechanisms for cooling, including refrigeration (Dumitru et al., 1991) and uplift-induced erosion (George and Dokka, 1994) resulting from subduction of a shallowly dipping buoyant Laramide slab must also be considered.

In this paper, we summarize our new geologic mapping, structural data, and ^{40}Ar/^{39}Ar thermochronometric studies of the Pinto shear zone in the New York Mountains of the northeastern Mojave Desert (Figs. 2 and 3). Previous workers have speculated that the Pinto shear zone is a Mesozoic thrust (Beckerman et al., 1982) or alternatively a Late Cretaceous normal fault (Miller et al., 1996); this discrepancy in part reflects the difficulty of distinguishing between extensional and contractional shear zones. To make this distinction and to resolve contrasting interpretations, we bring to bear a broad array of observations, including shear zone geometry and kinematics, hanging wall deformation style, progressive changes in deformation temperature, and differences in hanging wall and footwall thermal histories. From these data we conclude that the Pinto shear zone is an extensional shear zone of Late Cretaceous age. This shear zone lies intermediate between areas to the north and south in which latest Cretaceous extension has been previously documented. Contrary to the interpretation that 74–68 Ma cooling ages result from refrigeration of the Cordilleran lithosphere above a shallowly subducting Laramide slab (Dumitru et al., 1991) or erosional denudation (as suggested for the Peninsular Ranges; George and Dokka, 1994) we suggest that many of the Late Cretaceous cooling ages in the eastern Mojave Desert region result from post-intrusive cooling and exhumation by extensional structures. Late Cretaceous extension at 75–68 Ma was regional in scale in the southwestern Cordillera, and therefore requires a regional causative mechanism. We propose that Late Cretaceous extension of the Mojave sector of the Cordilleran orogen is most consistent with production of a low-viscosity lower crust during anatexis and/or removal of mantle lithosphere at the onset of Laramide shallow subduction.

2. Southern Cordilleran Mesozoic arc and thrust belt

The eastern Mojave Desert region is located at the site of intersection between the Mesozoic Cordilleran fold–thrust belt and the eastern fringe of the partly coeval, composite magmatic arc (Figs. 1 and 2). The magmatic arc rocks of the region include Jurassic plutonic and volcanic rocks (Glazner et al., 1994; Schermer and Busby, 1994; Fox and Miller, 1995; Gerber et al., 1995; Walker et al., 1995),
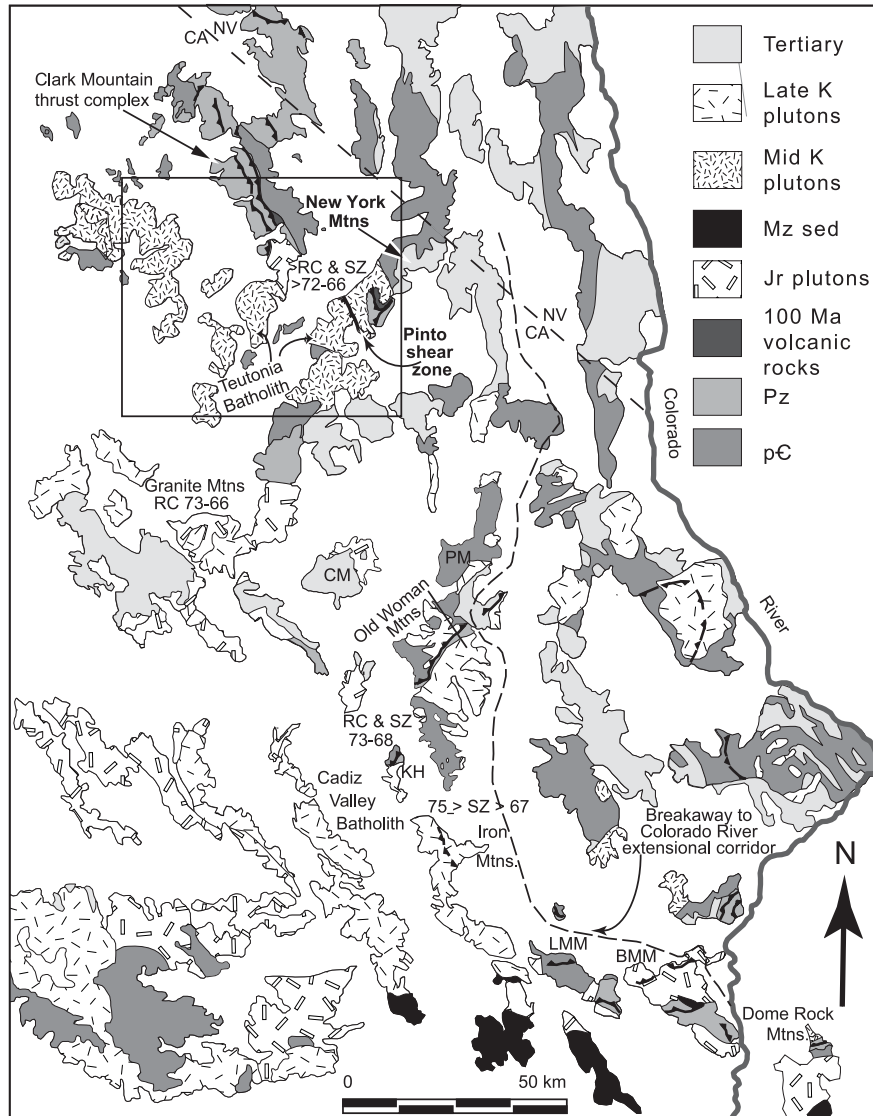
Fig. 2. Simplified geologic map of the eastern Mojave Desert of California and southern Nevada, showing location of the Pinto shear zone in the southern New York Mountains. The study area lies within the southern extension of the Clark Mountain thrust complex within the southern Cordilleran fold–thrust belt. Deformed roof rocks to the mid-Cretaceous Teutonia batholith display structures intermediate between thin-skinned styles to the north (eastern Clark Mountain thrust complex) and basement-cored nappes to the south (Old Woman and Big Maria Mountains). CM, Clipper Mountains; PM, Piute Mountains; KH, Kilbeck Hills; LMM, Little Maria Mountains; BMM, Big Maria Mountains. RC, rapid cooling; SZ, extensional shear zone activity; numbers in million years (Ma). Box shows location of Fig. 3. Modified from Jennings (1977), Howard et al. (1987), Miller et al. (1991) and Anderson et al. (1992).

mid-Cretaceous granitoids and minor volcanic rocks, and abundant Late Cretaceous metaluminous and peraluminous plutons (Armstrong and Suppe, 1973; Burchfiel and Davis, 1981; Beckerman et al., 1982; Foster et al., 1990; John and Mukusa, 1990; Fleck et al., 1994). The Teutonia batholith is one of the larger intrusive complexes in the eastern Mojave Desert (Figs. 2 and 3) and is comprised of 90–97 Ma metaluminous to weakly peraluminous granitic plutons (Beckerman et al., 1982; Anderson et al., 1992).

The Cordilleran fold–thrust belt is discontinuously preserved between the southernmost region of thin-skinned thrusting in the Clark Mountain thrust complex (Burchfiel and Davis, 1971) and the basement-involved fold nappes of the Big Maria and Dome Rock Mountains (Hamilton, 1987;

Boettcher and Mosher, 1998) of the Maria tectonic belt (Reynolds et al., 1986) (Fig. 2). Ductile fold nappes and thrusts within the Kilbeck Hills, Old Woman–Piute Mountains, and Clipper Mountains (Fig. 2) suggest substantial localized structural burial during the Mesozoic (Howard et al., 1987; Horinga, 1988; Fletcher and Karlstrom, 1990; Foster et al., 1992; Howard et al., 1995) and permit linking of the northern and southern contractile belts (Burchfiel and Davis, 1981).

3. Geology of the southern New York mountains

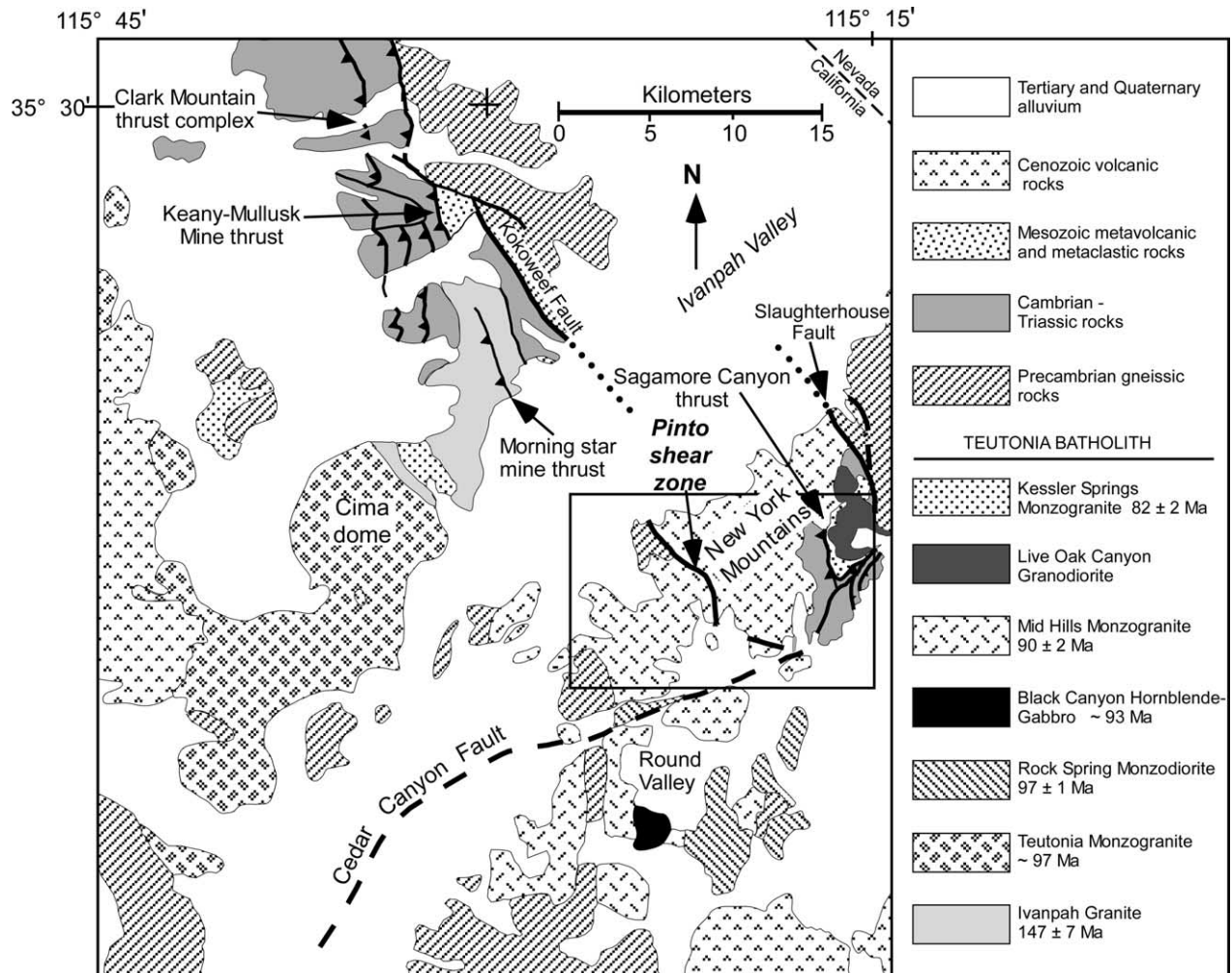Phanerozoic rocks are preserved along the eastern

Fig. 3. General geology of the Teutonia batholith and surrounding region. Note that Mesozoic structures of the Clark Mountain thrust complex correlate across the Ivanpah Valley to the New York Mountains: the Kokoweef fault to the Slaughterhouse fault, and the Keaney–Mullusk Mine thrust to the Sagamore Canyon thrust in the New York Mountains (Burchfiel and Davis, 1977; Smith et al., 2003). The Pinto shear zone lies in the hanging wall of the thrust stack exposed in the southeastern New York Mountains. Box shows location of Fig. 4. Modified from Beckerman et al. (1982) and Miller and Wooden (1993).

margin and within the roof of the Teutonia batholith in the southern New York Mountains, about 25 km southeast of the southern extent of the Clark Mountain thrust complex in the Mescal Range (Burchfiel and Davis, 1977; Beckerman et al., 1982) (Figs. 2–4). Substantial Mesozoic crustal thickening and attributes of both the northern and southern structural styles are evident; a stack of thrust duplications include Paleozoic over Mesozoic rocks, and Precambrian crystalline rocks are involved in map-scale folds (Burchfiel and Davis, 1977). The youngest low-angle fault that is clearly a thrust cuts 100 Ma metavolcanic rocks equivalent in age to the Delfonte volcanic rocks of the Mescal Range (Fleck et al., 1994; Smith et al., 2003) and predates intrusion of the Mid Hills monzogranite. These timing constraints are similar for the frontal thrust in the Clark Mountain thrust complex (Fleck et al., 1994; Walker et al., 1995).

The Teutonia batholith, as originally defined by Beckerman et al. (1982), is comprised primarily of early Late Cretaceous metaluminous to weakly peraluminous granitic

plutons with lesser Late Jurassic granitic rocks; a more restricted usage to include only Cretaceous intrusions was introduced by Anderson et al. (1992) and is adopted here. Several geochronological investigations have clarified the ages for some of the plutonic phases of the batholith but remaining ambiguities warrant additional work (Sutter, 1968; Beckerman et al., 1982; Dewitt et al., 1984; Walker et al., 1995; Miller et al., 1996). Two phases of the Teutonia batholith crop out in the New York Mountains: the Mid Hills adamellite of Beckerman et al. (1982), here called the Mid Hills monzogranite, and the Live Oak Canyon granodiorite of Beckerman et al. (1982) (Miller and Wooden, 1993). The Mid Hills monzogranite crops out over an area > 300 km^2 that extends from the eastern New York Mountains to the southern Mid Hills (Fig. 3), and intrudes Precambrian gneiss along its southern margin and both Paleozoic and Mesozoic metasedimentary rocks along its eastern margin. The Mid Hills monzogranite varies in mineralogy and texture and is probably a composite pluton.
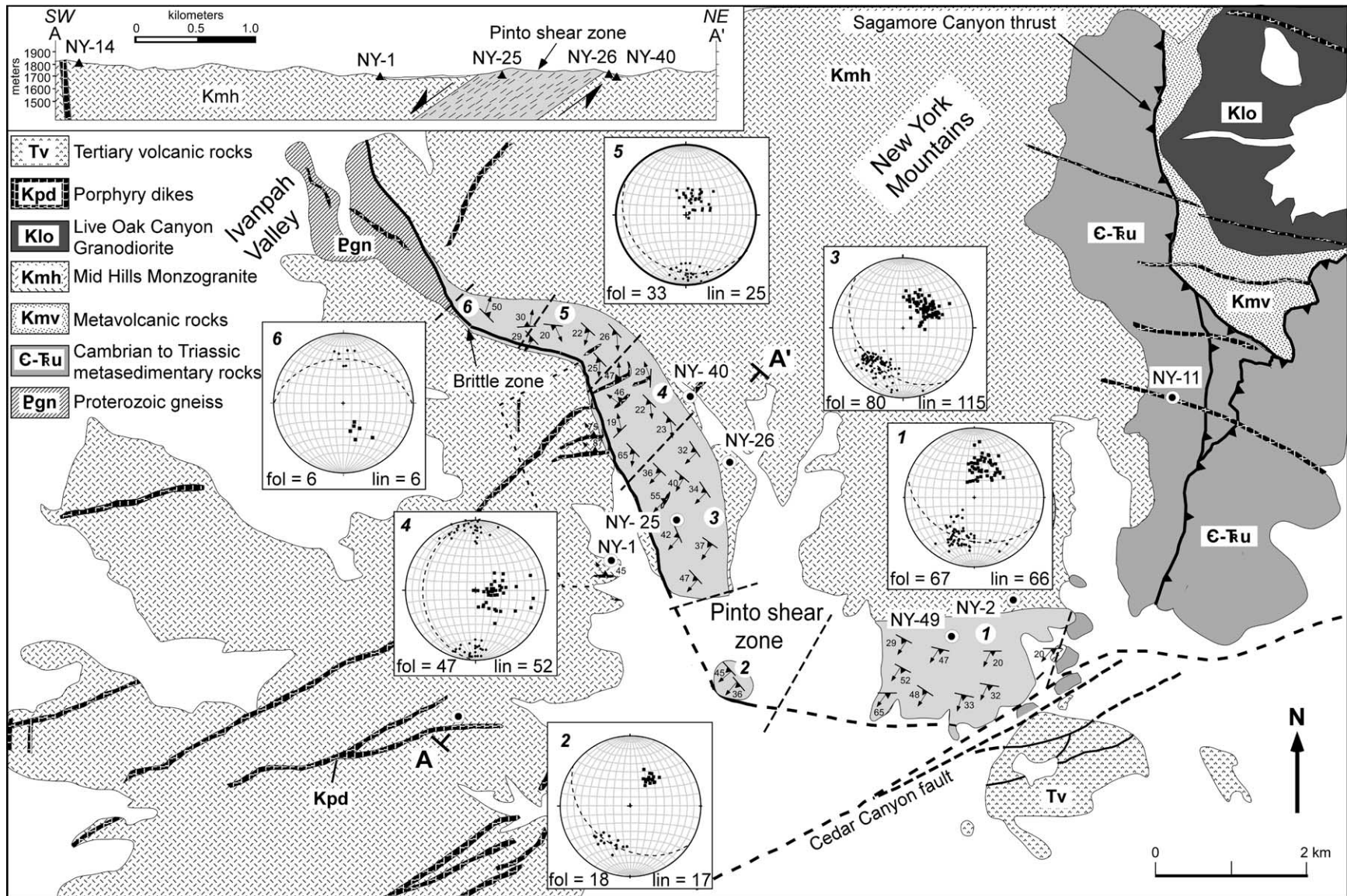
Fig. 4. Geologic and sample location map of the Pinto Valley area of the central New York Mountains, simplified from Miller et al. (1991), Burchfiel and Davis (1977), Beyene (2000) and Smith et al. (2003). Note overall Z-shaped map pattern to the Pinto shear zone and division of shear zone into six geometric structural domains (numbers on map, dashed lines represent domain boundaries), with corresponding stereograms of lineations (smaller circles), poles to foliation (larger boxes), and average foliation (dashed great circle). $^{40}Ar/^{39}Ar$ sample localities for samples reported here are shown, and U–Pb geochronology sample localities of Smith et al. (2003). The absence of mapped dikes in the central part of the map may reflect lack of detailed mapping. Area outlined by short dashed line in hanging wall above domains 3–5 represents study area of porphyry dikes. Inset: cross-section A–A′ along western thermochronology sampling transect, showing geometry of the shear zone and sample locations. Cross-section is of larger scale than map.

In Round Valley (Fig. 3), it has been dated at about 92 Ma by U–Pb on zircon (Miller et al., 1996), and recently at 88.2 + 1.6 Ma (1 sigma) by U–Pb SHRIMP on zircon (Barth et al., 2004). Smith et al. (2003) report an ion probe U–Pb zircon date of 90.0 ± 1.3 Ma (1 sigma) on the Mid Hills monzogranite in Pinto Valley (Fig. 4, location NY-1).

Numerous NE- to E-striking granodiorite porphyry dikes cut the Teutonia batholith and its country rocks and are more abundant near its roof and walls (Miller et al., 1996) (Fig. 4). The porphyry dikes in the New York Mountains have a distinctive texture and mineralogy including zoned K-feldspar, embayed quartz phenocrysts, and biotite in a fine-grained groundmass suggesting hypabyssal emplacement. Smith et al. (2003) report a U–Pb zircon date of 79.7 ± 3.6 Ma (1 sigma) for a porphyry dike south of Sagamore Canyon (Fig. 3; location NY-11), determined by TIMS on multigrain fractions. Recent ion microprobe analyses of zircon from this dike sample (Wells, unpublished data) indicate the presence of multiple inherited zircon fractions from older phases of the Teutonia batholith and a younger age of 74.6 ± 3.2 Ma for magmatic rims. This revised age is consistent with field relations; the dikes cut a pegmatite previously dated at 76–77 Ma by U–Pb zircon (Miller et al., 1996), in the Live Oak Canyon area of the New York Mountains.

4. The Pinto Shear zone

A mylonite zone first identified by Beckerman et al. (1982) and subsequently named the Pinto shear zone by Miller et al. (1996) crops out along the north side of Pinto Valley and continues northwest over the crest of the New York Mountains and into Ivanpah Valley (Figs. 3 and 4). The shear zone deforms the Mid Hills monzogranite and younger dikes and is truncated on the southeast by the Cenozoic Cedar Canyon fault and inferred to be truncated on the northwest by the Nipton fault in the subsurface of Ivanpah Valley (Miller et al., 1991, 1996). The shear zone strikes NW overall, but in detail has a Z-shaped map pattern (Fig. 4). With a thickness of about 550–600 m where mylonitic in the central part, the shear zone is thinner towards the north and ultimately grades northward into a 20-m-wide breccia zone; the brittle fault zone may have excised mylonitic rocks along the northern reaches of the shear zone. Deformation fabric in the central part generally increases structurally upward defining a strain gradient from undeformed granitoid in the footwall, through protomylonite, mylonite, to ultramylonite of variable thickness of 5–40 m at the top of the shear zone. Decameter-scale lenses of lesser-deformed rock that deviate from the strain gradient, however, are present within the shear zone. A brittle fault zone overprints the shear zone at variable levels near its top within the ultramylonite. Mylonite and ultramylonite zones are also developed along the margins of porphyry dikes in the hanging wall.

4.1. Kinematics and kinematic model

Kinematic studies were conducted on the Mid Hills monzogranite and porphyry dikes within the main shear zone and on discrete shear zones within the hanging wall, of which most are localized on the margins of porphyry dikes. Although sinuous in map pattern, foliation within the shear zone generally dips 20–65°S and SW, and lineation plunges SSW (Fig. 4). Kinematic studies of the Mid Hills monzogranite within the Pinto shear zone consistently yield non-coaxial top-to-the-SSW shear. Shear sense indicators are abundant, and all indicators including S–C fabrics (Berthe et al., 1979; Lister and Snoke, 1984), mica fish (Lister and Snoke, 1984), winged feldspar porphyroclasts (Passchier and Simpson, 1986), myrmekite quarter structures (Simpson and Wintsch, 1989), C′-type shear bands (Passchier and Trouw, 1996), and oblique dynamically recrystallized quartz grain-shape (Law et al., 1984; Lister and Snoke, 1984) show top-to-the-SSW sense of shear (Fig. 5(a)–(d)).

The deformation of porphyry dikes varies across the Pinto shear zone and imposes important constraints on its kinematic evolution. A geometric and kinematic analysis of the dikes was conducted in an area of the hanging wall west of structural domains 3–5 of the shear zone (Fig. 4). The majority of porphyry dikes within the hanging wall are E- and NE-striking (Fig. 4), steeply N-dipping (40–75°) and exhibit localized mylonite to ultramylonite along their margins. A solid-state foliation is subparallel to the dike margins, and lineation is generally down-dip and varies from 312°/63° (trend/plunge) to 350°/39° (Fig. 6a). Sense-of-shear indicators (Fig. 5e and f), including ubiquitous biotite fish, record a consistent down-to-the-NNW shear, antithetic to the shear in the rest of the Pinto shear zone. A few dikes are N-striking and steeply dipping; these contain shallowly plunging lineation and record dextral shear (Fig. 6a). Several porphyry dikes in the hanging wall can be traced downwards across the upper shear zone boundary and into ultramylonitic rocks. The dikes are progressively thinned and deflected towards parallelism with c-surfaces of the ultramylonite as they cross the shear zone downwards, and a transition from down-to-the-NNW to top-to-the-SW shear is noted with increasing deformation of the dike. Overprinting relationships between these oppositely directed fabrics are not apparent.

Within the shear zone (domains 3–5), the porphyry dikes are of variable orientation and accommodate both synthetic and antithetic shear relative to the main shear zone (Figs. 6b and 7). Within the central part of the shear zone, dikes striking E to NNE with a component of north dip, exhibit a solid-state foliation throughout their widths and a north trending lineation. Kinematic studies of the dikes show antithetic down-to-the-N shear throughout their widths and, weak to moderately developed SW-dipping foliation within the monzogranitic country rock shows an apparent deflection into parallelism with the dike margin as the
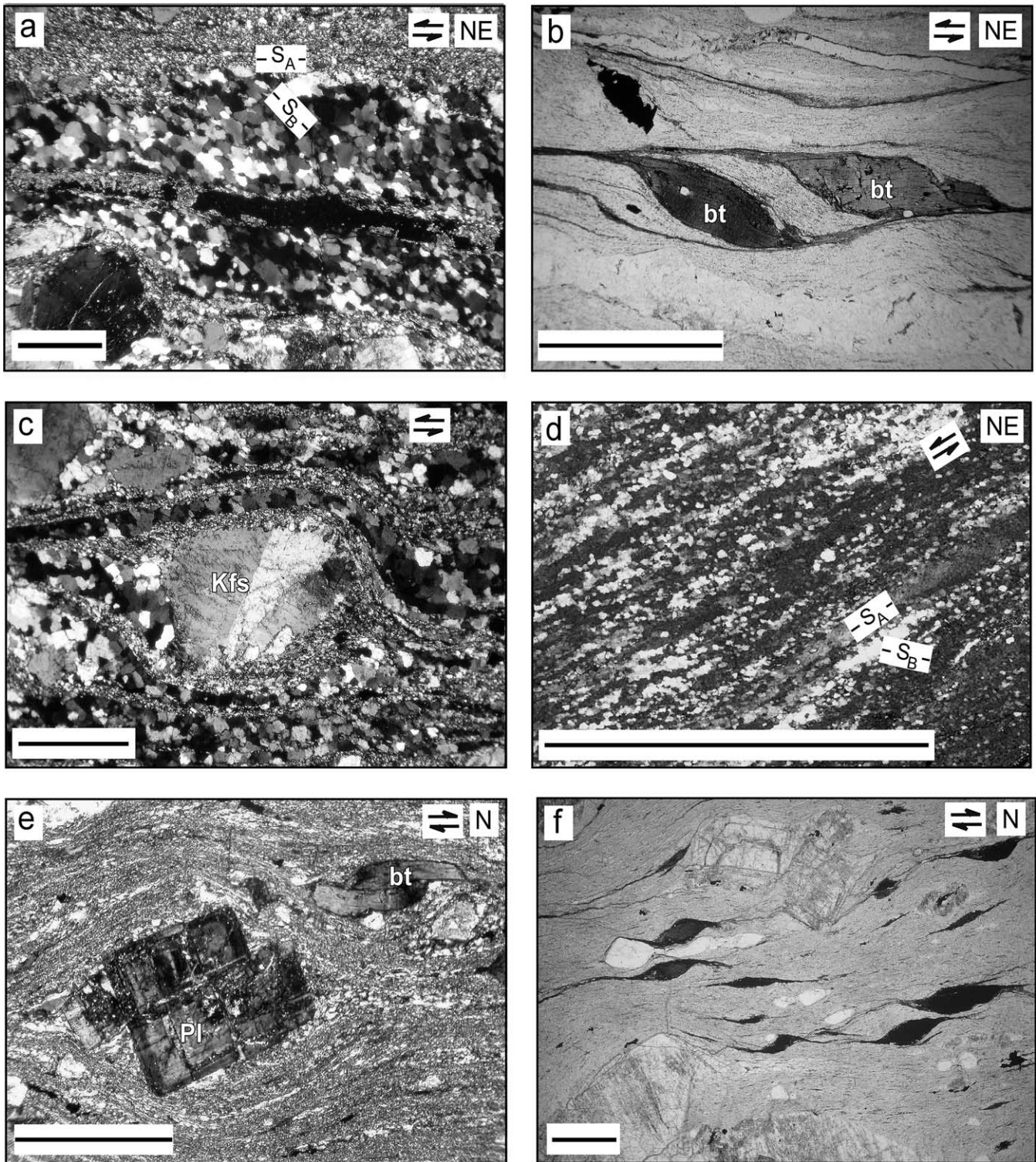
Fig. 5. Kinematic indicators from the Pinto shear zone ((a)–(d)), and from the antithetically-sheared porphyry dikes ((e) and (f)). (a) Oblique grain-shape fabric in dynamically recrystallized quartz. S_A is defined by mica-rich zones of concentrated strain parallel to quartz ribbons and S_B is defined by the long axis of dynamically recrystallized quartz grains (Law et al., 1984). (b) Biotite (bt) fish from deformed porphyry dike in the central part of the shear zone. (c) σ-Type K-feldspar porphyroclast showing top-to-the-SW (sinistral) sense of shear. (d) Deformed quartz vein shows elongate quartz ribbons (S_A) and oblique grain-shape fabric (S_B) of dynamically recrystallized quartz. (e) Synthetic rotation resulting from antithetic microfracturing along the cleavage of plagioclase feldspar in porphyry dike, indicating top-to-the-N (dextral) sense of shear. Note synthetic shearing of biotite fish along basal cleavage. (f) Mica fish in porphyry dike, indicating dextral (top-to-the-N) sense of shear. Scale bar, one millimeter.
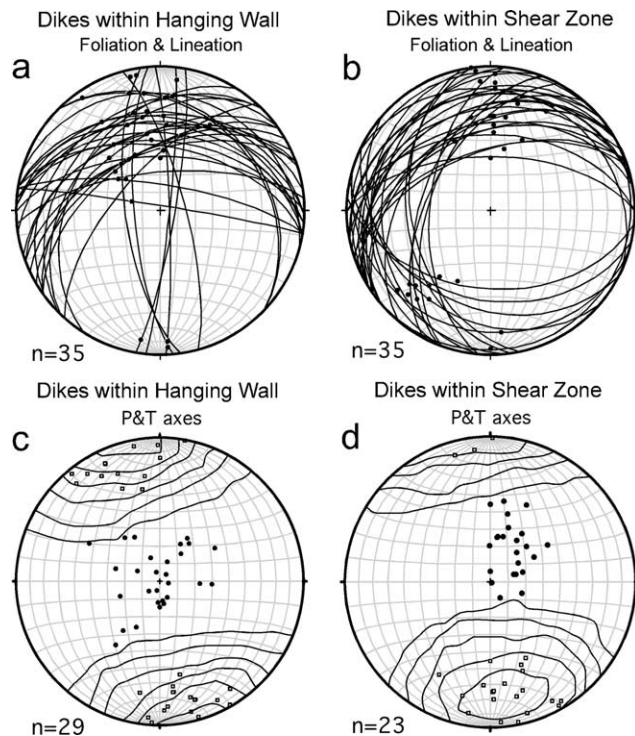
Fig. 6. Kinematic analysis of porphyry dikes. Foliation tends to parallel the dike margin and serves as a proxy for dike orientation. (a) Foliation and lineation in porphyry dikes of the hanging wall adjacent to domains 4 and 5 of shear zone. Note two orientation populations: (1) the predominant NE- to NW-striking, N-dipping dikes, and (2) the subordinate N-striking, sub-vertical dikes. North-dipping dikes show antithetic top-to-the-N shear, and N-striking dikes show dextral shear. (b) Foliation and lineation within porphyry dikes within the shear zone. Dikes are in three principal orientations: (1) E-striking and north dipping, (2) E-striking and south dipping, and (3) N-striking and west dipping. S-dipping dikes show top-to-the-SW shear (synthetic), N-dipping dikes show antithetic top-to-the-N shear, and N-striking dikes show dextral-normal shear. (c) and (d) 'P' (infinitesimal shortening, filled circles) and 'T' (infinitesimal extension, open squares) axes determined for antithetic shears along N-dipping dike margins; contours are of 'T' axes by Kamb method.

strain intensity increases, compatible with the determined shear sense (Fig. 7). The dikes are progressively rotated with increasing amount of antithetic shear within the dike and increasing amount of synthetic shear in the country rock. Where the dikes are W- to NW-striking with a component of south dip, typically within more highly strained parts of the shear zone, they record top-to-the-SW sense of shear synthetic to the shear in the surrounding mylonitic monzogranite. In general, the lineation in the dikes within the shear zone have similar trend to the local monzogranitic mylonite (compare Figs. 4 and 6b). Porphyry dikes in the footwall are undeformed, and dikes cannot be continuously mapped across the shear zone to assess total displacement.

Two observations are critical to deciphering the relative timing between down-to-the-N shear along the dike margins and top-to-the-S shear within the Pinto shear zone. (1) The porphyry dikes in the hanging wall exhibit down-to-the-N kinematics and are progressively deformed and rotated downwards into the ultramylonite zone, and where

significantly thinned and rotated, exhibit top-to-the-S shear: continuations of zones of down-to-the-N shear through the ultramylonite are not apparent (Fig. 7). (2) Foliation in lesser-deformed lenses in Mid Hills monzogranite within the shear zone show abrupt increases in intensity in concert with progressive rotation into parallelism with the margin of N-dipping dikes that exhibit antithetic shear throughout their widths (Fig. 7). The simplest interpretation that reconciles these two relationships of relative timing is that the antithetic high-angle normal sense shears were broadly active simul-taneously with top-to-the-S shear along the main zone.

The similarity in azimuths of movement direction inferred from the lineation within the dike-margin shears in the hanging wall, deformed porphyry dikes within the shear zone, and the mylonite and ultramylonite derived from monzogranite within the shear zone support this view by suggesting kinematic compatibility (Figs. 4 and 6). This can be further appreciated by consideration of the similarity in best-fit kinematic axes of infinitesimal extension for the antithetic shearing in the hanging wall (Fig. 6c) to those within the shear zone (Fig. 6d), determined using the fault-slip kinematic analysis approach of Marrett and Allmen-dinger (1990) (FaultKin 4.1X; Allmendinger, 2001).

Internal rotation of hanging wall blocks synthetic to the main shear zone was accomplished by synchronous antithetic slip along high-angle normal shears, which were influenced by the orientation and spacing of the dikes (Fig. 7). Dike margins in the hanging wall along the range crest 3 km to the west, and along the mountain flank on the east side of Ivanpah Valley, including some of the same continuous dikes that show down-to-the-N shear closer to the roof of the shear zone, do not exhibit solid-state foliation at their margins. As dictated by strain compatibility, the shear must terminate at an upper boundary analogous to a kink band, separating rocks that rotated during shearing from rocks that did not (Fig. 7). The kinematics of synthetic block rotation both within the shear zone and the hanging wall was influenced by the orientation of the dikes. The localization of antithetic shearing along the dike margins suggests that the porphyry dikes, with their fine-grain groundmass, represented weak zones along which defor-mation was localized. The anisotropy due to their systematic orientation controlled the style of synthetic block rotation. A similar geometry is described within a Miocene extensional shear zone in the Sacramento Mountains of the Colorado River trough region (Pease and Argent, 1999; Stewart and Argent, 2000). In the Sacramento Mountains, antithetic shear, localized along dikes, accommodated synthetic rotation of blocks.

It is interpreted that the porphyry dikes intruded along parallel, or perhaps en-échelon extension fractures during generally N–S extension within the Teutonia batholith and its wall rocks. The U–Pb age of 74.6 ± 3.2 Ma for the porphyry dikes permits intrusion to have occurred prior to or during early movement along the shear zone. While the fine-grained groundmass of the dikes suggests hypabyssal
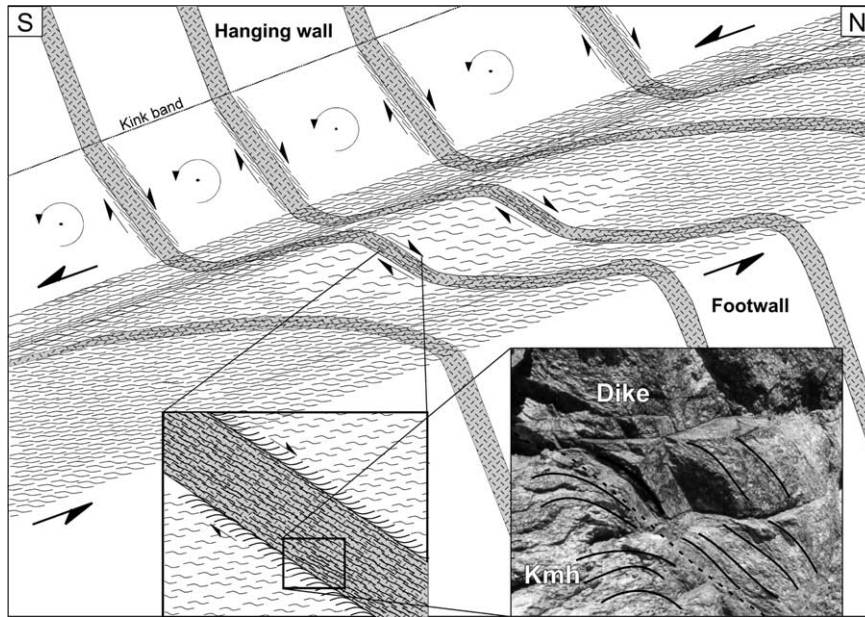
Fig. 7. Schematic model showing deformation style of the Mid Hills monzogranite and porphyry dikes within the Pinto shear zone and hanging wall. Steep shear zones antithetic to the principal shear sense are localized along porphyry dikes and bound blocks that experienced rotation synthetic to the principal shear sense, requiring an upper kink-band boundary. Lesser-deformed lenses within the shear zone experienced thinning by antithetic motion along shear zones localized within porphyry dikes. Inset in lower right shows view of the margin of an E-striking, N-dipping porphyry dike within the shear zone, looking W. Dashed line is dike margin, solid lines are form lines of foliation.

emplacement, depth estimates independent of the cooling histories are not available to allow the depth of the Mid Hills monzogranite, prior to dike emplacement, to be assessed. We note that the dikes strike WNW where mapped in the footwall of the Pinto shear zone in the Live Oak Canyon area, but strike NE in the hanging wall (Fig. 4); while this difference in orientation is probably original, it cannot be ruled out that a component of vertical axis rotation was accomplished along the shear zone.

4.2. Deformation mechanisms

Study of deformation mechanisms from microstructures within the Mid Hills monzogranite show an apparent decrease in temperature during progressive shearing, from plastic deformation at upper greenschist to lower amphibolite facies conditions to brittle deformation conditions. K-feldspar displays abundant evidence for early dynamic recrystallization followed by later cataclasis. K-feldspar is dynamically recrystallized at porphyroclast tails (Fig. 8a–c), which extend into layers defining mylonitic foliation (Fig. 8a). Strain-induced myrmekite (quartz + plagioclase) growth is ubiquitous on K-feldspar grain boundaries that are facing the inferred incremental shortening direction, and dynamic recrystallization of myrmekite was apparently an important matrix-producing mechanism as bands of micron-sized quartz + plagioclase alternate in the matrix with quartz ribbons and bands of dynamically recrystallized K-feldspar (Fig. 8b and c). New K-feldspar is locally grown in dilatant sites including micro pull-aparts and strain shadows. These

microstructures and mineral reactions most probably occur in K-feldspar in the temperature range of 450–550 °C (Simpson and Wintsch, 1989; FitzGerald and Stünitz, 1993; Pryer, 1993; Passchier and Trouw, 1996). Deformation continued at somewhat lower temperature conditions as indicated by flame perthite, undulose extinction, and kink bands in K-feldspar (∼350–450 °C) (Pryer, 1993). Tensile fractures cut K-feldspar cores, dynamically recrystallized new grains and myrmekite, and are infilled with muscovite + quartz (Fig. 8c). The brittle deformation overprint on early plastic features is greatest near the top of the shear zone, and grain size reduction by fracture suggests temperatures <350 °C (±50). Where Paleozoic carbonate is present in the immediate hanging wall, extensive secondary retrograde alteration and mineralization accompanied cataclasis, and fine-grained epidote and chlorite filled and sealed fractures and cataclastic crush zones of fine-grained angular fragments, and calcite locally replaced plagioclase (Fig. 8d).

Quartz also shows evidence for dynamic recrystallization during decreasing temperature conditions. At lower structural levels in the shear zone completely recrystallized quartz ribbons (Type 2a of Boullier and Bouchez, 1975) with interlobate grain boundaries indicate dominantly high-temperature grain boundary migration recrystallization (Stipp et al., 2002). These grains are locally overprinted by pervasive low-T plasticity including deformation lamellae. In other samples, particularly at higher structural levels within the shear zone, progressive development of subgrains and new grains within and around larger quartz
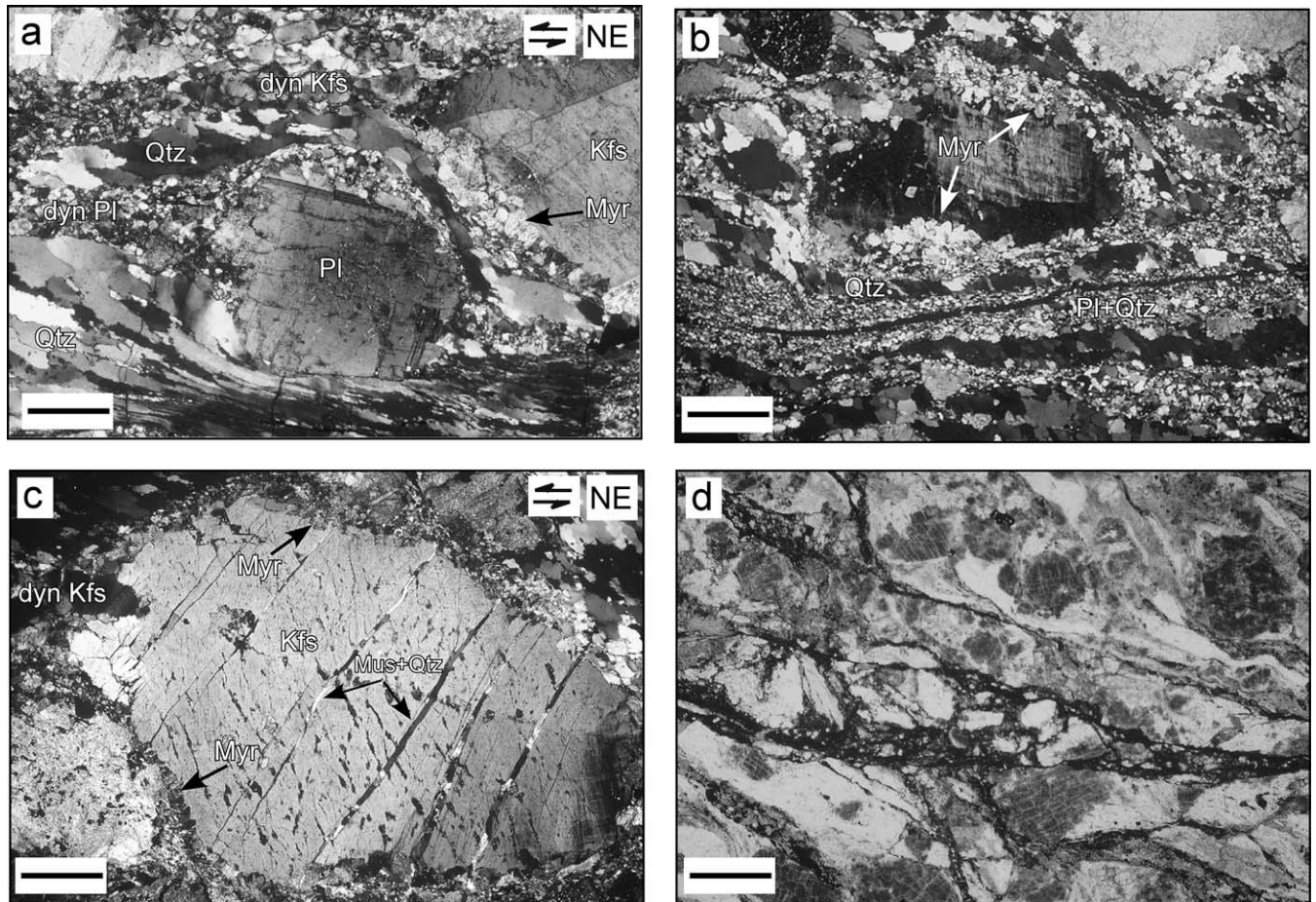
Fig. 8. Microstructures illustrating deformation mechanisms in the Mid Hills monzogranite. (a) Sigma-shaped plagioclase (Pl) porphyroclast with mantle (upper margin) and tails of fine-grained dynamically recrystallized grains (dyn Pl). Tail of K-feldspar porphyroclast in upper right is dynamically recrystallized and forms more coarse grained band (dyn Kfs) extending to left. (b) K-feldspar porphyroclast with extensive myrmekite (Myr) formation on upper right and lower left margins. Note banding defined by alternating layers of quartz ribbons (Qtz) and fine-grained feldspar and quartz. Textural relations suggest that myrmekite sited on K-feldspar porphyroclasts is progressively dynamically recrystallized and forms fine-grained bands in matrix. (c) K-feldspar porphyroclast with extension fractures that cut clast, marginal myrmekite, and dynamically recrystallized K-feldspar in tails. Fractures are filled by muscovite + quartz. (d) Fault rock from brittle fault capping ultramylonite. Fine-grained epidote and chlorite fill and seal fractures and cataclastic crush zones of fine-grained angular fragments. Scale bar, one millimeter.

ribbons suggests subgrain-rotation recrystallization correlative to regime 2 of Hirth and Tullis (1992) (Stipp et al., 2002) (Fig. 5d). Quartz ribbons are cut by extension fractures filled by muscovite and quartz, indicating a superposition of brittle ($<300\,°C$) on plastic fabrics.

5. ^{40}Ar/^{39}Ar Thermochronology

Seven samples were collected from the footwall, hanging wall, and within the shear zone for ^{40}Ar/^{39}Ar thermochronology along two transects, to be referred to as the eastern and western transects (Fig. 4). In total, five muscovites, three biotites, and four K-feldspars were analyzed. Sample locations are shown in Fig. 4. A description of the laboratory procedures (Appendix A), the ^{40}Ar/^{39}Ar data tables (Appendix B), Ca/K plots (Appendix C) and isochron plots for micas (Appendix D) are available as electronic supplements. Results are presented

in Figs. 9–12. Data are presented at the one-sigma level of uncertainty.

5.1. Muscovite and biotite

5.1.1. Western transect

Muscovite in the three samples of Mid Hills monzogranite occurs dominantly as secondary (hydrothermal or metamorphic) grains in variably oriented microscopic fractures within mineral grains of the monzogranite, with lesser magmatic muscovite. Muscovite (NY-1M) from the hanging wall of the Pinto shear zone (Fig. 4) shows a stair-stepped age spectrum with ages increasing from 68.0 ± 0.4 to 74.4 ± 0.4 Ma with increasing temperature and a total gas age of 72.0 ± 0.4 Ma (Fig. 9a). Coexisting biotite (NY-1B) yields a discordant age spectrum with a slight saddle at intermediate temperature steps, and a total gas age of 71.2 ± 0.4 Ma.

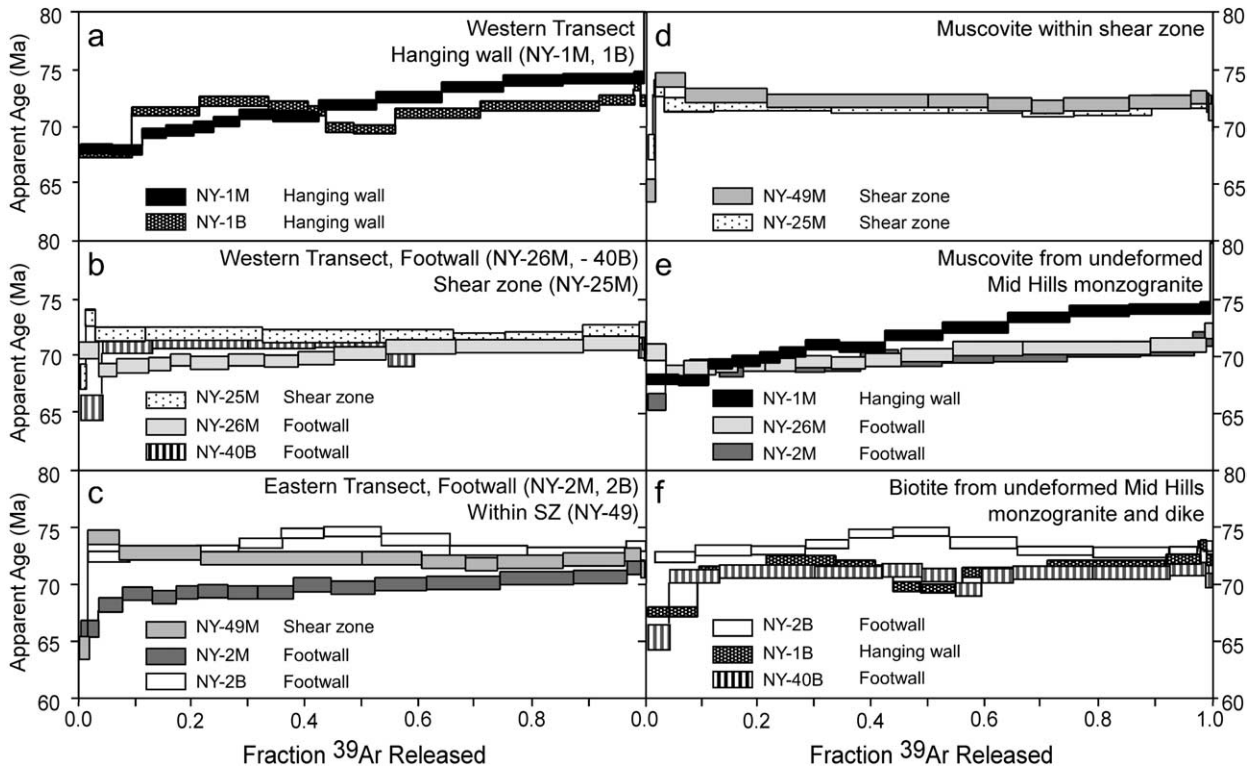Muscovite (NY-25M) was analyzed from a quartz vein

Fig. 9. The $^{40}Ar/^{39}Ar$ apparent age spectra of muscovite (M) and biotite (B) from the Pinto Valley area. (a) Muscovite and biotite (NY-1, Mid Hills monzogranite) from the hanging wall of the Pinto shear zone along the western transect. (b) Muscovite (NY-26, Mid Hills monzogranite) and biotite (NY-40, porphyry dike) from the footwall and muscovite (quartz vein) from within the shear zone from the western transect. (c) Muscovite and biotite from the eastern transect. (d) Comparison between muscovite from aplite and quartz vein within the shear zone. (e) Comparison between muscovite from the Mid Hills monzogranite. (f) Comparison between biotite from the Mid Hills monzogranite.
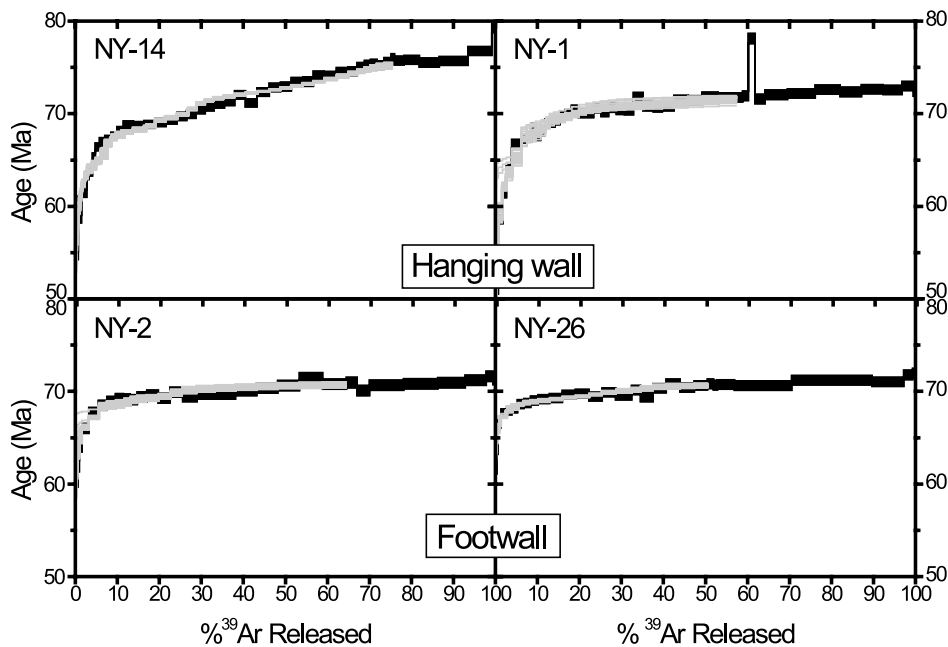

Fig. 10. The $^{40}Ar/^{39}Ar$ apparent age spectra of K-feldspar. Modeled age spectra, following the approach outlined in the text and Fig. 11, are shown in grey scale. Note excellent fit between model and measured age spectra.
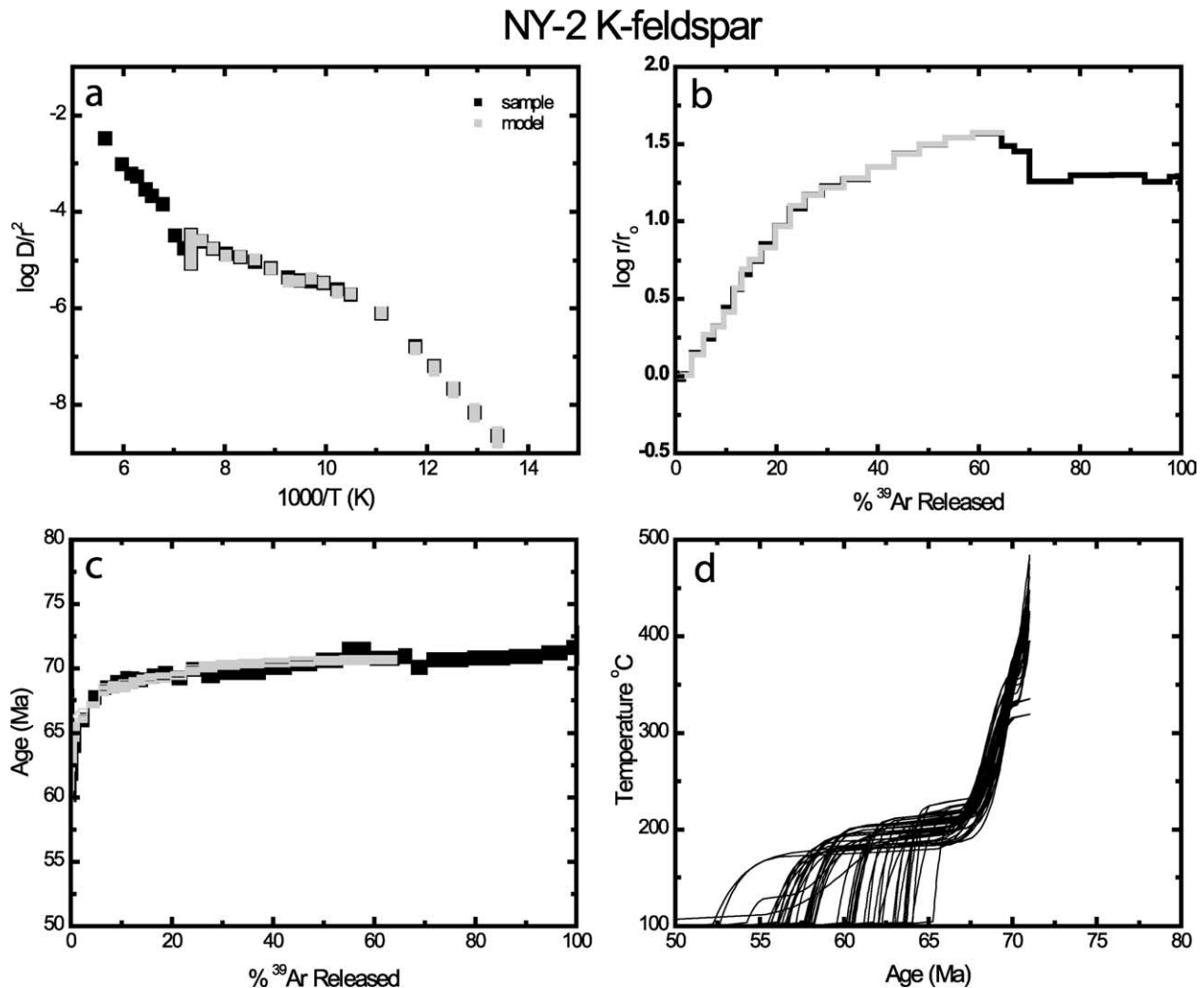
NY-2 K-feldspar

Fig. 11. Multiple diffusion domain modeling of K-feldspar from the Mid Hills monzogranite. Example shown is NY-2 from the footwall of the Pinto shear zone; all samples produced equally good agreement between modeled and experimentally derived (a) Arrhenius parameters and (b) logr/r_o plots. (d) Fifty cooling histories determined from 10 E–D_o pairs. The distribution of the 50 calculated cooling histories for each sample reflects the uncertainty in the obtained activation energies. Model age spectra (c) are produced by cooling histories (d) shown.

within the shear zone (Fig. 4). This quartz vein is weakly deformed and exhibits large quartz grains with serrate grain boundaries leading to the development of new smaller grains by grain boundary migration recrystallization, a bimodal grain size and a lattice-preferred orientation. Muscovite occurs in grain clusters and has a weak preferred orientation. This sample produced a flat age spectrum, with a plateau age of 71.9 ± 0.3 Ma (Fig. 9b), indistinguishable from the total gas age of 71.9 ± 0.4 Ma and isochron age of 72.0 ± 0.8 Ma (MSWD$=1.7$).

Muscovite (NY-26M) from the Mid Hills monzogranite in the footwall of the Pinto shear zone (Fig. 4), similar to NY-1M, occurs dominantly as secondary grains with lesser magmatic muscovite. The sample yielded a slight age gradient from 68.9 ± 0.6 to 72.4 ± 0.6 Ma (Fig. 9b) and a total gas age of 70.4 ± 0.4 Ma. Biotite lacking chemical alteration and suitable for analysis from the footwall in the western transect was only found in an undeformed porphyry

dike that intrudes the Mid Hills monzogranite. Biotite (NY-40B) shows a flat age spectrum with a plateau age of 71.0 ± 0.4 Ma, indistinguishable from the total gas age of 70.9 ± 0.4 Ma (Fig. 9b).

5.1.2. Eastern transect

Cenozoic sedimentary and volcanic rocks cover the hanging wall in the southeastern part of the shear zone. Samples were collected from within the shear zone and from the undeformed footwall.

Muscovite (NY-49M) from a mylonitic alaskite dike within the shear zone (Fig. 4) yields a flat age spectrum and plateau age of 72.3 ± 0.3 Ma (Fig. 9c), a total gas age of 72.4 ± 0.4 Ma and an isochron age of 72.8 ± 0.4 (MSWD$=$1.07). Unlike muscovite from the main phase of the Mid Hills monzogranite, muscovite NY-49M is entirely of igneous origin and helps to define the mylonitic foliation.

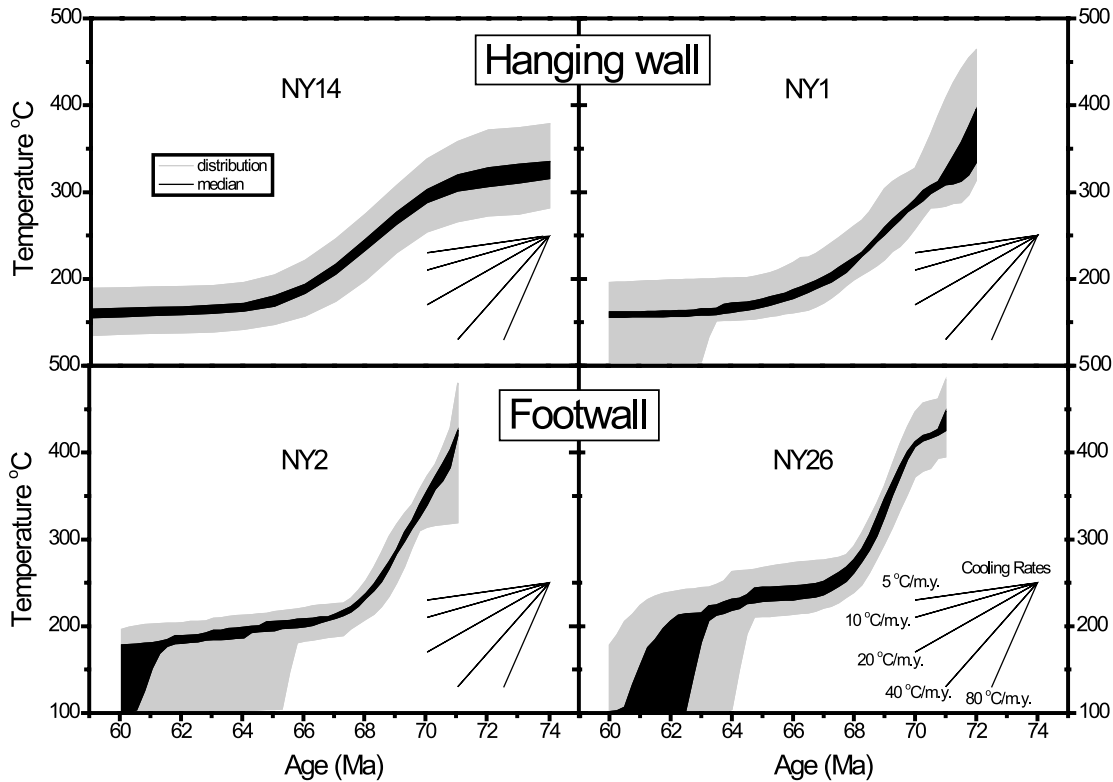Muscovite (NY-2M) from the Mid Hills monzogranite in

Fig. 12. Summary of cooling histories determined from MDD modeling of K-feldspar. Grey pattern, 90% confidence intervals for the total distribution, and black, 90% confidence for the median of the distribution (Lovera et al., 1997).

the footwall (Fig. 4) produced an age spectrum with an age gradient from 66.3 ± 0.8 to 71.7 ± 0.6 Ma (Fig. 9c). Muscovite NY-2M, similar to other muscovite separates from the Mid Hills monzogranite (NY-1M and NY-26M) occurs dominantly as secondary (hydrothermal or metamorphic) grains within microscopic fractures. Coexisting biotite (NY-2B), of igneous origin, yields a discordant age spectrum with an intermediate hump, with all heating steps (excluding the first) between 72.5 and 74.7 Ma but no plateau, and a total gas age of 72.8 ± 0.4 Ma (Fig. 9c). The sample does not yield a statistically valid isochron age. However, isochron regression analysis suggests the presence of excess argon.

5.2. K-feldspar

K-feldspars were analyzed using detailed furnace step heating including isothermal duplicates to obtain diffusion properties $(E, D_o/r_2)$ for application of the multiple diffusion domain (MDD) modeling approach of Lovera et al. (1989, 1991). Calibration of the furnace was accomplished via a double thermocouple experiment in which the actual sample position (inner crucible) temperature and time history was recorded during step heating cycles at different temperatures (as measured by the outer control thermocouple). Inner crucible temperatures and times for heating steps were used in modeling. Activation energy (E) was determined using a least squares linear regression of data from low-temperature steps of the experiment plotted on an Arrhenius diagram

(Lovera et al., 1989). The frequency factor (D_o) for each diffusion domain was determined using the calculated activation energy and modeling the Arrhenius plot (Lovera, 1992). Ten $E–D_o$ pairs were then randomly selected from a Gaussian distribution around the values and their uncertainties obtained from the Arrhenius diagram (Lovera et al., 1997). For each pair, a single activation energy was assumed to be representative of all domains used in the modeling. The number of domains along with their size and volume fraction was modeled using a variational iterative technique to determine the best fit between the experimental and modeled results on a domain size distribution plot [$\log(r/r_o)$ vs. %^{39}Ar released] (Richter et al., 1991). Five cooling histories were then determined for each $E–D_o$ pair by fitting modeled age spectra to the experimental age spectrum using these parameters and domain distributions. The cooling histories obtained were then used to calculate 90% confidence intervals for the total distribution and median of the distribution (Lovera et al., 1997).

Two separates of K-feldspar at similar depths beneath the Pinto shear zone (NY-26K and NY-2K, western and eastern transects, respectively; Fig. 4), and two from the hanging wall (NY-1K and NY-14K, western transect; Fig. 4) 500 m and 2 km structurally above the top of the shear zone, were analyzed and modeled to construct thermal histories; all samples are from the Mid Hills monzogranite. The age spectra for all K-feldspar are shown in Fig. 10; an example of the modeled Arrhenius, domain distribution, age

spectrum, and cooling history plots are shown in Fig. 11 of K-feldspar NY-2K; the complete modeling results for the other three K-feldspars are available as an electronic supplement in Appendix E; the resulting model cooling histories are presented in Fig. 12. The Arrhenius and domain distribution plots of the samples and the models produced very good to excellent fits (Fig. 11), indicating that the diffusion properties determined in the laboratory data approximate those acting in the sample when in the natural geological environment, and that the furnace temperature is stable and well calibrated. The four K-feldspar age spectra show very similar forms, with steep age gradients in the first 10–15% ^{39}Ar released rolling over into shallow age gradients in the remainder of the analyses (Fig. 11). The K-feldspars in this study are not affected by excess argon, as indicated by comparison between calculated K-feldspar closure temperatures and muscovite and biotite cooling ages, analysis of the argon isotopic ratios using inverse isochrons, and the lack of a decrease in age in the second of the isothermal duplicate heating steps. Therefore, the K-feldspar samples are ideal for thermal modeling.

The activation energies determined for the four K-feldspars range from 46.1 ± 2.7 to 52.7 ± 5.0 kcal/mol for the hanging wall samples (NY-1 and NY-14, respectively) and 58.7 ± 5.8 to 50.5 ± 2.4 kcal/mol for the footwall samples (NY-26 and NY-2, respectively). The modeled cooling curves for the two footwall K-feldspars define average cooling rates of 62 °C/m.y. (NY-2K) and 76 °C/m.y. (NY-26K) from 71 to 68 Ma (Fig. 12). The hanging wall K-feldspars produced modeled cooling curves with cooling rates of 33 °C/m.y. (NY-1K) and 28 °C/m.y. (NY-14) from 72 to 66 Ma.

5.3. Interpretation of mica age spectra

The stair-stepped age spectra of the muscovite from the Mid Hills monzogranite (Fig. 9a–c and e) may be interpreted as either slow (NY-1) or moderately slow (NY-26M and NY-2M) cooling through the closure temperature interval for muscovite, or a mixture of radiogenic argon from hydrothermal and igneous muscovite, representing a mixing between growth and cooling ages, respectively. We favor a mixed age origin for the age gradients, with younger ages at lower experimental temperatures corresponding to gas release from hydrothermal muscovite, because: (1) petrographic examination shows the presence of both hydrothermal and igneous muscovite, although in varying abundance between samples; (2) the apparent ages for the lower furnace-temperature portions of the age gradients are younger than apparent ages for coexisting and adjacent biotite as well as muscovite from alaskite and quartz veins within the shear zone (Fig. 9b and c) and K-feldspar ages for domains with closure temperatures similar to micas ($\sim$ 300–400 °C); (3) apparent K–Ca ratios (Appendix C) of muscovite are more highly variable for the samples from the Mid Hills

monzogranite (NY-1M, NY-2M, and NY-26M) than for the quartz vein or alaskite (NY-25 and NY-49); (4) the cooling rates determined from modeled retentive footwall K-feldspar shows a relatively rapid, not slow, cooling rate of 62–76 °C/m.y. that encompasses a portion of the closure temperature interval for muscovite; and (5) preservation of growth ages for hydrothermal muscovite is consistent with the inferred temperatures for fracturing. The fractured K-feldspar in the shear zone is surrounded by plastically deformed quartz, and fractures are filled with quartz + muscovite, which implies that a component of deformation occurred within the 400–250 °C temperature range (Hirth and Tullis, 1992; FitzGerald and Stünitz, 1993; Pryer, 1993). If the muscovite growth in fractures in the shear zone is coeval with muscovite growth within fractures in the footwall and hanging wall, then it follows that footwall muscovite growth occurred within the temperature range of 250–400 °C, consistent with the ages recording growth and not cooling. Furthermore, the age gradient may predominantly reflect progressive growth of hydrothermal muscovite during deformation (e.g., Kirschner et al., 1996), with the majority of radiogenic argon evolved from hydrothermal grains. Hydrothermal muscovite growth occurred during cooling and inferred exhumation, and if the latter interpretation is correct, was apparently synchronous in the two footwall sample localities, as indicated by the similarity in morphology between the two footwall muscovite age spectra (Fig. 9e).

In summary, the mica ^{40}Ar/^{39}Ar results are consistent with 74–72 Ma cooling of igneous mica followed by 72–69 Ma growth of hydrothermal muscovite during cooling. Despite the differences in detail, the similarity in ages indicate that cooling of igneous mica and growth of muscovite in fractures occurred during a relatively short time interval within the period of rapid cooling shown by the K-feldspar MDD modeling.

6. Discussion

6.1. Does the Pinto shear zone record extension or shortening?

Previous workers have speculated that the Pinto shear zone is a Mesozoic thrust (Beckerman et al., 1982) or alternatively a Late Cretaceous normal fault (Miller et al., 1996). This discrepancy in part reflects the difficulty of distinguishing extensional from contractional shear zones, perhaps one of the foremost challenges in structural studies, and in particular in deformed intrusive complexes that lack useful stratigraphic or metamorphic relationships between the hanging wall and footwall. To distinguish an extensional from a contractional origin for the Pinto shear zone and resolve the contrasting interpretations we bring to bear a broad array of observations including shear zone geometry and kinematics, hanging wall deformation style, progressive

changes in deformation temperature, and differences in hanging wall and footwall thermal histories; we conclude that the Pinto shear zone is a ductile normal fault.

6.1.1. Shear-zone geometry and kinematics

Shear-sense indicators within the Mid Hills monzogranite consistently demonstrate top to-the-SSW, generally down-dip shear sense consistent with normal-sense motion in the present geographic coordinates. The foliation in the shear zone varies in its dip from 20 to 65°SW. The possibility of tilting (to the SW) a NE-dipping thrust fault by more than 65° is considered unlikely, as suggested by geologic relations in the Live Oak Canyon area, 7 km to the NE (Fig. 4). The Live Oak Canyon granodiorite intrudes into the base of a Cretaceous volcanic succession, concordant to the overlying low-angle Sagamore Canyon thrust, which it deforms into a structural dome (Burchfiel and Davis, 1977; Smith et al., 2003). These relationships are most consistent with a position in the roof of a pluton (laccolith) rather than a pluton sidewall, suggesting no large magnitude post-intrusion tilt.

6.1.2. Hanging wall kinematics

The geometric and kinematic relationships between top-to-the-SW shearing within the main shear zone and antithetic high-angle shears localized at dike margins within the hanging wall are most compatible with extensional rather than contractional motion along the Pinto shear zone. The antithetic high-angle shears extend the hanging wall and merge downward with the top of the main shear zone, and are interpreted as developing synchronously with the main shear zone (Fig. 7). Normal faults that merge downwards with detachment faults and occur in their hanging walls are very common in metamorphic core complexes and detachment fault systems (e.g. Crittenden et al., 1980; Stewart and Argent, 2000). Although normal faults that developed coevally with and soling into major thrust zones have been documented (Yin and Kelty, 1991), these examples are few and are associated with contractional structures such as minor thrusts, folds and cleavage and may record a part of the non-coaxial strain field in the base of the thrust sheet. No contractional structures have been documented either in the footwall or hanging wall of the Pinto shear zone that postdate the intrusion of the Mid Hills monzogranite and interact with the shear zone, or that postdate the Cretaceous phases of the Teutonia batholith in the larger region (Fig. 3).

6.1.3. General-shear thinning of shear zone

In addition to thinning of the hanging wall, the main shear zone was also thinned during deformation as shown by the synthetic rotation of antithetically sheared N-dipping porphyry dikes (Fig. 7). Thus, the bulk flow within the shear zone was general shear (e.g. Simpson and DePaor, 1993) in which the coaxial component accomplished shortening perpendicular to the shear-zone boundary and extension parallel to the boundary and in the shear direction. The folding of dikes that cross foliation at a high angle and strike parallel to the transport direction, about axes parallel to the shear direction, also record shortening perpendicular to the shear-zone boundary. While thinning shear zone behavior is not diagnostic of ductile normal faults as opposed to thrusts, vorticity studies of extensional shear zones commonly show such thinning shear-zone behavior (Lee et al., 1987; Wallis, 1992; McGrew, 1993; Wells, 2001; Bailey and Eyster, 2003).

6.1.4. Footwall and hanging wall thermal histories

Thermal modeling and thermochronometric studies have shown that the hanging walls and footwalls to both thrust and normal faults experience markedly different thermal histories. One- and two-dimensional thermal models of normal faults suggest that footwalls experience rapid cooling rates during and following rapid faulting (Ruppel et al., 1988; Grasemann and Mancktelow, 1993; Ketcham, 1996); rapid cooling documented by numerous thermochronometric studies of the footwalls of detachment faults fit these models well (e.g. Hoisch et al., 1997; Foster and John, 1999; Wells et al., 2000). The thermal history of hanging walls to detachment faults have received less attention, but several one- and two-dimensional thermal modeling studies show that hanging walls may experience heating due to juxtaposition against a hot footwall if the advection of heat in the footwall is sufficient due to rapid displacement (Grasemann and Mancktelow, 1993; Dunkl et al., 1998). Cooling, as the geothermal gradient reequilibrates, is predicted to follow reheating after the cessation of slip. In contrast, the footwalls to thrusts should experience heating during or following thrusting with peak temperatures following the cessation of thrusting (England and Thompson, 1984; Ruppel and Hodges, 1994), whereas hanging walls should experience cooling during erosional denudation concurrent with rock uplift and slip.

In the construction of cooling histories for the footwall and hanging wall of the Pinto shear zone, we have not explicitly integrated the mica ^{40}Ar/^{39}Ar results but rather have relied upon the MDD modeling of the K-feldspar argon data. The K-feldspar MDD modeling procedure is robust in extracting meaningful cooling histories from well-behaved K-feldspars such as those from the Mid Hills monzogranite, as the diffusion parameters for each individual K-feldspar separate can be measured directly and the uncertainty in estimation of these parameters can be propagated into the determination of cooling history (Lovera et al., 1997; Fig. 12). The analyzed K-feldspars were relatively retentive to argon diffusion, resulting in cooling histories that reached or spanned the commonly assumed 'nominal' closure temperatures for muscovite and biotite (McDougall and Harrison, 1999). The uncertainties in estimating closure temperatures for the micas of this study are significant resulting from a number of factors including the difficulty in extracting the kinetic parameters of diffusion from hydrous
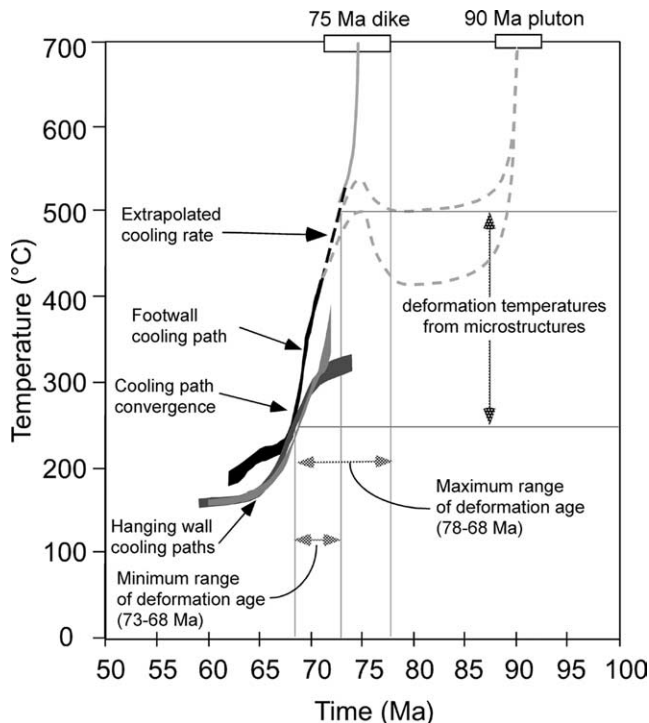
Fig. 13. Synoptic diagram of constraints on the timing of deformation within the Pinto shear zone. Dashed grey lines depict two of many possible pre-extensional cooling histories for the 90 Ma Mid Hills monzogranite, differing in depth of emplacement and extent of Late Cretaceous heating. Cooling paths determined from K-feldspar MDD modeling are shown. Open boxes indicate U–Pb zircon ages. Microstructures suggest deformation began at ∼500 °C and continued to cataclastic conditions at <250 °C.

minerals, potential compositional control on argon diffusion and uncertainties in the effective diffusion radius (McDougall and Harrison, 1999, and references therein). Furthermore, there is petrographic and isotopic evidence for two populations of muscovite in the samples from the Mid Hills monzogranite. It should be noted, however, that for samples exhibiting a single mica population (NY-40B and NY-49M), by assuming that the physical grain size represents the effective diffusion dimension and using the fast cooling rates as determined by the MDD modeling of K-feldspar, calculated closure temperatures are significantly higher than 'nominal' temperatures, making their placement in T–t space consistent with the K-feldspar MDD modeled cooling histories.

The difference in the cooling rates and positions of the cooling paths for the hanging wall and footwall of the Pinto shear zone supports an extensional interpretation (Fig. 13). The two footwall samples cooled at rates of 62 and 76 °C/m.y. whereas the two hanging wall samples cooled at about 50% of those rates, 28 and 33 °C/m.y. The cause of cooling of the hanging wall will be discussed further in Section 6.3.

6.1.5. Deformation during decreasing temperature conditions

Microstructural studies indicate that the bulk of the distributed deformation occurred at upper and middle greenschist facies conditions, with temperatures decreasing during deformation, as shown by kinematically compatible brittle deformation overprints on early plastic deformational features—in particular for feldspar. This superposition of lower temperature on higher temperature deformation is interpreted to have occurred during the progressive unroofing of the footwall block. Such decreasing temperature conditions during progressive shearing are commonly observed in extensional shear zones (Lister and Davis, 1989) and are predicted by thermal models (Grasemann and Mancktelow, 1993; Ketcham, 1996).

The new kinematic and deformation-mechanism studies presented here provide a compelling case in support of the reinterpretation of the Pinto shear zone as an extensional shear zone (Miller et al., 1996), which requires revision in the existing correlation of faults across the Ivanpah Valley. The Pinto shear zone was previously interpreted as a thrust fault (New York Mountain thrust of Beckerman et al. (1982)) and correlated across the Ivanpah Valley to the Morning Star thrust (Burchfiel and Davis, 1971) of the southern Ivanpah Mountains (Fig. 3). Subsequent kinematic studies of the west-dipping Morning Star thrust have confirmed thrust-sense, top-to-the-E kinematics (Sheets, 1996). The recognition that the Pinto shear zone records top-to-the-SW normal-sense motion, rather than top-to-the-E thrusting, precludes the correlation of these faults. Below we more explicitly discuss the geochronologic and thermochonologic data that constrains the Pinto shear zone as Late Cretaceous in age.

6.2. Age of the Pinto shear zone

The timing of motion along the Pinto shear zone is well constrained by the combination of U–Pb crystallization ages (Smith et al., 2003), the thermal history of footwall rocks derived from $^{40}Ar/^{39}Ar$ thermochronology, and microstructural studies. The shear zone deforms 74.6 ± 3.2 Ma (U–Pb, zircon) porphyry dikes, which provides a maximum age on deformation; however, the dikes may have intruded early in the extensional history. Microstructural studies indicate that the bulk of the distributed deformation occurred at upper and middle greenschist-facies conditions, with temperatures decreasing during deformation down to cataclastic conditions. The cooling history of the footwall is well defined by the MDD modeling results of two K-feldspars, which shows rapid cooling from 420 to 220 °C over the time interval 71–68 Ma. Consideration of the deformation temperatures, in conjunction with the cooling history, indicates that much of the ductile fabric was acquired between >71 and 68 Ma (Fig. 13). An abrupt reduction in footwall cooling rates at 67–68 Ma is coincident with a convergence in the cooling paths for the footwall and hanging wall, and is interpreted to indicate the end of cooling resulting from exhumation by the Pinto shear zone

(Figs. 12 and 13). This reduction in cooling rate may postdate the actual reduction or termination of slip due to the time lag for thermal re-equilibration of the advected isotherms (Ketchum, 1996). An alternative to the apparent reduction in cooling evident from the modeling, which assumed monotonic cooling, is that the age gradient in the low-T portion of the K-feldspar age spectra results from a moderate reheating. However, Paleocene to early Eocene reheating in this region has not been recognized. Constraining the age of initiation of extension is more difficult without higher temperature thermochronology (e.g. hornblende) or a more accurate constraint on the age of the dikes. Extrapolating the 62–76 °C/m.y. footwall cooling rate to the higher temperatures present during initial shearing, as inferred by the K-feldspar plasticity and myrmekite formation, suggests early higher temperature shear initiated before ∼72 Ma (Fig. 13). Therefore, extensional motion on the shear zone initiated between 78 (maximum age of dike; Fig. 13) and 72 Ma, and was over by 68 Ma.

6.3. Mechanisms to explain hanging wall cooling

An unexpected result of this study is the relatively rapid cooling rate determined for the hanging wall and the lack of significant discordance in mica ages between hanging wall and footwall. Below we discuss several possible explanations including: (1) refrigeration of the lithosphere by shallow Laramide subduction; (2) heating of the hanging wall by the hot footwall, and subsequent cooling, sympathetic but slower than in the footwall; (3) cooling of the hanging wall due to an unrecognized structurally higher coeval normal fault; and (4) cooling following heating resulting from intrusion of a pluton at depth.

Dumitru et al. (1991) proposed that the shift from normal to shallow subduction during the Laramide orogeny caused widespread refrigeration of the North American lithosphere in the western Cordillera, including the eastern Mojave Desert region. During low-angle subduction, the western Cordillera may have developed a much colder, forearc-like thermal structure due to refrigeration of the lithosphere by the relatively cool underlying subducting slab that displaced hotter mantle asthenosphere. The refrigeration effect is hypothesized to have migrated eastward through time along with the eastward propagating low-angle slab, with refrigeration in the eastern Mojave Desert region (Old Woman and Chemehuevi Mountains) beginning ca. 68 Ma (fig. 4 of Dumitru et al., 1991). This shift from an arc-like to forearc-like geotherm could have important thermal and rheological effects in the western Cordillera, including strengthening and increased resistance to gravitational collapse. Refrigeration and strengthening coeval with extension thus seems implausible. Therefore, it is unlikely that the rapid cooling evident in the hanging wall and footwall of the Pinto shear zone, which was synchronous with extensional shearing along the zone, is related to

Laramide refrigeration. However, refrigeration is a viable explanation for post-68 Ma cooling, after the convergence of cooling paths for the hanging wall and footwall (Fig. 13), and may have contributed to the cessation of Late Cretaceous extension.

Alternatively, cooling of the hanging wall may record thermal relaxation following heating due to juxtaposition against a hot footwall. Such reheating, followed by cooling, is predicted by two-dimensional thermal modeling and has been documented by low-temperature thermochronology and thermal-maturation studies of the hanging wall to the Rechnitz Window of the eastern Alps (Dunkl et al., 1998). The similarity of the footwall mica ages and the mica ages from the base of the hanging wall, 500 m above the shear zone, supports the interpretation that the hanging wall was heated by juxtaposition against a hot footwall, perhaps aided by fluid advection during shearing as suggested by widespread secondary mineralization of muscovite and quartz in the hanging wall, footwall, and within the shear zone. Such heating would be followed by relatively rapid cooling of the hanging wall, as the geothermal gradient relaxed following the cessation of slip. This mechanism for hanging wall heating followed by cooling may explain the difference in modeled K-feldspar cooling histories between the samples 500 m and 2 km from the fault, but cannot explain the cooling evident 2 km above the fault (NY-14). Two-dimensional finite difference thermal modeling indicates that the thermal anomaly across the fault is not of sufficient magnitude to provide significant heat conduction across 2 km of the hanging wall; therefore, an additional mechanism is needed to explain the thermal history of NY-14.

Cooling of the hanging wall may be caused by tectonic denudation along a now exhumed and eroded structurally higher normal fault that once projected above the study area. Although no such structures are present between the shear zone and the Cenozoic alluvium of Ivanpah Valley, an unrecognized extensional structure may exist further to the west. Late Cretaceous cooling of mid-crustal granites in the Granite Mountains to the southwest (Fig. 2) (Miller et al., 1996; Kula et al., 2002) requires an unrecognized exhumational structure of similar age to the Pinto shear zone; this structure may have projected above the New York Mountains.

Finally, a portion of the Late Cretaceous cooling may result from cooling, following heating, resulting from intrusion of a large Cretaceous pluton at depth. The widespread occurrence of 74–80 Ma dikes in the area allows this possibility. Such conductive cooling, following heating in the roof of a pluton would allow for the relatively rapid cooling rates seen in the hanging wall to the shear zone.

To conclusively distinguish between the remaining potential causes for cooling of the hanging wall block—a structurally higher normal fault, thermal effects following juxtaposition against a hot footwall, or conductive cooling

in the roof of a pluton—additional thermochronological studies, coupled with thermal modeling, from a variety of structural levels within the hanging wall and from the larger region are required. However, despite the uncertainty in explanation of cooling of the hanging wall, the fundamental conclusion of this study is not diminished—a large component of shearing within the Pinto shear zone occurred during rapid cooling in the Late Cretaceous.

6.4. The cause of Late Cretaceous extension and peraluminous magmatism in the eastern Mojave

The established Late Cretaceous age and extensional origin for the Pinto shear zone allows its integration with other structures of similar age and kinematic significance in the eastern Mojave Desert and southern Great Basin, to provide a framework for evaluating the cause for initiation of synconvergent extension in the southwestern Cordillera. Hodges and Walker (1992) reviewed evidence for early Cretaceous to Paleocene extension within the interior of the Cordilleran orogen, from northern Washington to southern California. Subsequent studies, outlined below, in the eastern Mojave Desert have confirmed the importance of Cretaceous extension in the evolution of the orogen and allow for a better definition of its age and continuity.

An extensional origin and Late Cretaceous age for mylonitic gneiss in the roof zone of the Cadiz Valley batholith in the Iron Mountains (Fig. 2) (Miller and Howard; 1985) has been established (Wells et al., 2002). A systematic decrease in biotite $^{40}Ar/^{39}Ar$ cooling ages in the transport direction beneath a >1.3 km thick stack of top-to-the-E mylonitic rocks indicates extensional shearing bracketed between crystallization of porphyritic monzogranite (75 ± 2, U–Pb zircon) and muscovite and biotite $^{40}Ar/^{39}Ar$ ages of 67–69 Ma (Wells et al., 2002). Concordant magmatic and solid-state foliations and synmagmatic shearing fabrics suggest synextensional pluton emplacement. Similar timing for extensional shearing and intrusion is recorded in the Old Woman Mountains (Fig. 2). Synmagmatic deformation within the Old Woman pluton (74 ± 3 Ma; Foster et al., 1989), and solid-state mylonitic deformation within the pluton and wall rock screens, record $\sim$E–W extension and vertical shortening (McCaffrey et al., 1999). When combined with earlier studies, including those of the western Old Woman Mountain shear zone, it is apparent that extension was active from intrusion at 74 Ma to $^{40}Ar/^{39}Ar$ muscovite closure at 68 Ma (Carl et al., 1991; Foster et al., 1992; McCaffrey et al., 1999). Rapid exhumation of mid-crustal rocks in the Granite Mountains of the Mojave National Preserve (Fig. 2) has been documented by barometry, geochronology, and thermomochronology of 75–76 Ma granites. Al-in hornblende geobarometry indicates intrusion at $\sim$4.5 kbar followed by rapid cooling through hornblende $^{40}Ar/^{39}Ar$ closure interpreted as rapid conductive cooling to country rock temperatures (Kula, 2002; Kula et al., 2002). Continued

rapid cooling from 350 to 60 °C from 73 to 68 Ma, as shown by K-feldspar MDD and apatite fission track-length modeling, is interpreted as resulting from tectonic exhumation (Kula et al., 2002). Metamorphic rocks in the Funeral Mountains of the Death Valley region (Fig. 1) were exhumed along the Cenozoic Boundary Canyon detachment fault (Wright and Troxel, 1993; Hoisch and Simpson, 1993); however, an earlier history of partial exhumation along the Monarch Canyon and Chloride cliff shear zones has been suggested (Applegate et al., 1992; Applegate and Hodges, 1995). The age of deformation is constrained by U–Pb dating of synkinematic pegmatite (72 ± 1 Ma, zircon) and postkinematic pegmatite (70 ± 1 Ma, zircon) (Applegate et al., 1992). Extension of this age may be more widespread in the Death Valley region: a shear zone in the Panamint Range at an equivalent stratigraphic position to the Chloride Cliff shear zone, the Harrisburg fault (Hodges et al., 1990; Andrew, 2001), may also be Late Cretaceous. Based on these examples and the constraints provided by the Pinto shear zone, extension was apparently widespread in the narrow time interval between 75 and 68 Ma along the axis of the southwestern Cordilleran orogen.

These sites of Late Cretaceous extension all have early- to syn-extensional plutons or dikes that are part of the belt of Late Cretaceous granites of the Cordilleran interior (Figs. 1 and 2), dominantly of strongly peraluminous compositions (Miller and Barton, 1990; Barton, 1990; 'Cordilleran peraluminous granites' of Patiño Douce (1999)). These rocks have isotopic signatures consistent with variable sources in Precambrian continental basement and are widely attributed to be products of crustal anatexis (Farmer and DePaolo, 1983; Miller, 1985; Patiño Douce et al., 1990; Wright and Wooden, 1991). A mantle component to these magmas has also been suggested as experimental studies implicate hybridization of basaltic melts through interaction with Precambrian metagreywacke (Patiño Douce, 1999), and field observations, although uncommon, provide evidence for interaction between felsic and mafic magmas (Foster and Hyndman, 1990; Kapp et al., 2002). These granites are largely restricted to areas underlain by Precambrian basement that has undergone Mesozoic shortening. While crustal thickening was certainly a necessary precondition for melting (Patiño Douce et al., 1990), additional factors required for anatexis are controversial, including: fluid infiltration into hot crust from a shallow Laramide slab (Hoisch, 1987; Hoisch and Hamilton, 1990), increased mantle heat flux (Armstrong, 1982; Barton, 1990), heating through mafic magmatic underplating or intrusion, or decompression melting (Hodges and Walker, 1992; Harris and Massey, 1994). The common association between peraluminous plutons and extension is suggestive of either a causal relationship or a shared root cause. Decompression melting is excluded for a number of reasons (Barton, 1990) including the observation here that extension is syn-emplacement to post-emplacement, but not pre-emplacement to plutons.

Synconvergent extension, in theory, may have been driven by either a reduction in horizontal compressive stress transmitted across the Farallon–North American plate boundary and/or basal décollement to the Cordilleran orogen, or an increase in forces resulting from lateral contrasts in gravitational potential energy. Because the Farallon–North American plate relative convergent velocity increased in the Late Cretaceous (Engebretson et al., 1985), as did the predicted buoyancy of the subducted slab (Henderson et al., 1984), synconvergent extension due to slab rollback (Royden, 1993) is precluded. We see two explanations for synorogenic extension, although not mutually exclusive, as compatible with the observations from the southwestern Cordillera: (1) decoupling of the middle to upper crust from the mantle lithosphere by development of a low-viscosity lower crust, allowing lateral contrasts in gravitational potential energy to relax by extensional flow, and (2) removal of mantle lithosphere, thereby increasing the lateral contrast in potential energy.

Widespread melting and attendant lowering of the viscosity of the lower crust, required in the production of Cordilleran peraluminous granites, may have played a role in initiating synconvergent extension in the southwest Cordillera. Experimental petrology and petrochemical modeling of the peraluminous granites require a deep crustal source (Patiño Douce, 1999; Kapp et al., 2002). The site of melting was most probably diffuse and sheet-like as it was controlled by the thermal and lithologic structure of the lithosphere (Sawyer, 1998). A reduction in strength during partial melting of the lower crust has the effect of decoupling the overlying crust from the underlying mantle, effectively insulating the crust from stresses due to plate coupling, thus removing the lateral support and allowing the overlying crust to respond to lateral gradients in gravitational potential energy (Vanderhaeghe and Teyssier, 2001). If extension occurred after the low-angle slab made contact with eastern Mojave continental lithosphere, fluid infiltration from a dewatering Farallon slab could have further weakened the lower crust (Malin et al., 1995).

Widespread Late Cretaceous heating, anatexis, magmatism, and extension may have been promoted by removal of mantle lithosphere prior to 75 Ma, either prior to the arrival of a flat slab beneath the eastern Mojave region or during its initial impingement (Fig. 14). The removal of lithospheric mantle by delamination (Bird, 1979) or convection (Houseman et al., 1981; England and Houseman, 1988) has been proposed as an effective mechanism to dramatically increase the gravitational potential energy of a
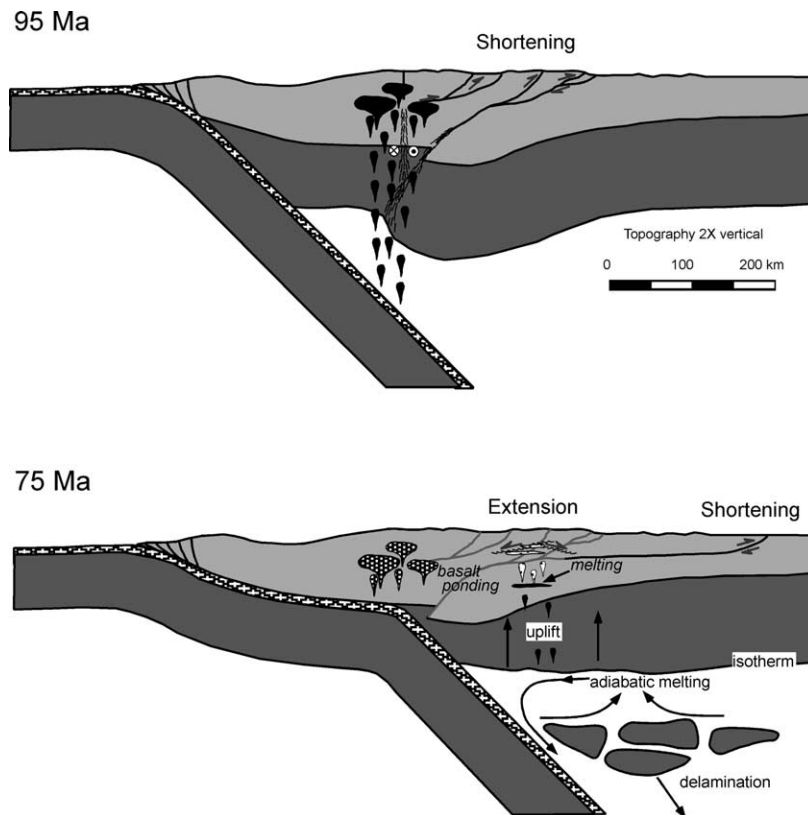

Fig. 14. Tectonic cartoon for Late Cretaceous removal of mantle lithosphere. A significant root of mantle lithosphere developed due to Sevier orogenesis—mass balance (strain compatibility) requires shortening of mantle lithosphere equivalent in magnitude to shortening of crust in fold–thrust belts of the Mesozoic backarc. Instability of thickened mantle lithosphere leads to delamination causing: adiabatic melting of asthenosphere, transfer of heat into lower crust resulting from basalt intrusion and conductive heating of thinned lithosphere, crustal melting and magmatism, buoyancy-driven uplift, and gravitationally-driven extension.

mountain belt and promote surface uplift and horizontal extension. Removal of lithospheric mantle results in an increase in Moho temperature and geothermal gradient, and may produce mafic magmatism through adiabatic decompression of asthenosphere (Platt and England, 1993; Kay and Kay, 1993; Kay and Abbruzzi, 1996). This process would provide the additional heat necessary for crustal anatexis, and heat transfer could be rapid if by basaltic intrusions (Leventhal et al., 1995; Annen and Sparks, 2002). We are not explicit in addressing the mechanism by which the lithosphere may have been removed during the onset of the Laramide orogeny. Removal of mantle lithosphere, whether by delamination (Bird, 1979), convective removal (England and Houseman, 1988) or viscous ablation, produces a similar response of heating and buoyancy of the remaining lithosphere, and thus a first order understanding of the responses (i.e. extension, crustal melting) is not reliant on the details of the mechanism of removal. Delamination and lower crustal weakening are not necessarily separate and alternative mechanisms, but may have worked together to create the rheological and dynamic state necessary to extend the crust.

Delamination is proposed here to have occurred immediately before eastward propagation of low-angle subduction of the Farallon plate, during the inception of the Laramide orogeny. The recognition of a thin and fertile Archean mantle lithosphere beneath the eastern Mojave from xenolith studes (Lee et al., 2001) shows a dense mantle lithosphere capable of density-driven foundering and thickness compatible with prior removal. Removal of lithosphere was required to allow flattening of the slab to achieve a low-angle geometry, and we suggest that delamination, whether piecemeal or involving larger blocks of foundered lithospheric mantle, took place before the asthenospheric mantle wedge was expelled. The presence of asthenospheric mantle wedge beneath the eastern Mojave prior to 75 Ma allows displacement of detached lithosphere via counterflow, and upwelling of asthenosphere to produce basaltic melts (Leventhal et al., 1995). Lithosphere removal by delamination, rather than subduction-erosion, allows the underplating of water-rich metasediments, as evident in the tectonic windows of the Rand–Pelona–Orocopia schist belt (Jacobsen et al., 1996). Furthermore, the presence of asthenospheric mantle during lithosphere removal allows the North American lithosphere to be isostatically independent of the load of the Farallon slab, rather than isostatically coupled, and to uplift rather than subside (Cross and Pilger, 1978; Bird, 1984). Delamination or detachment of lithospheric mantle explains many enigmatic yet prevalent aspects of the metamorphic, magmatic, and kinematic history of the southwestern Cordilleran orogen.

7. Conclusions

The following observations are used to establish that the Pinto shear zone is a Late Cretaceous extensional shear zone rather than a ductile thrust. (1) Foliation in the Pinto shear zone generally dips 20–65°S and SW with lineations plunging to the SSW, and kinematic studies consistently demonstrate top-to-the-SSW shearing. (2) The hanging wall of the Pinto shear zone, and low-strain domains within the shear zone, were extended by synthetic rotation of blocks bound by antithetic north-dipping normal-sense shear zones localized along the margins of or within porphyry dikes. Structural relationships between these antithetic shear zones and the main shear zone indicate simultaneous displacement. (3) Differential cooling rates are evident between hanging wall and footwall. Cooling rates constrained by K-feldspar $^{40}Ar/^{39}Ar$ MDD modeling are 62–76 °C/m.y. for the footwall and 28–33 °C/m.y. for the hanging wall. (4) Microstructural studies indicate deformation during decreasing temperatures, from lower amphibolite–upper greenschist facies to cataclastic conditions, interpreted to record progressive unroofing of the footwall block during an enigmatic 'regional' cooling as evident by moderate cooling rates of the hanging wall.

The timing of extension is well constrained by the combination of a U–Pb crystallization age on deformed porphyry dikes and integration of estimated deformation temperatures with the dated thermal history. Deformation of 74.6 ± 3.2 Ma porphyry dikes together with a reduction in cooling rate at 67–68 Ma, marking the termination of rapid cooling related to tectonic denudation, brackets extension between <78 and 68 Ma. The cooling history of the hanging wall close to the shear zone (500 m) and similarity between ages of hydrothermal muscovite in the footwall and hanging wall suggest conductive heating of the hanging wall by the hot footwall aided by fluid advection, and consequent sympathetic but slower cooling than the footwall. However, the relatively rapid cooling experienced by the hanging wall at greater distances from the shear zone ($\sim$2 km) requires an additional mechanism for cooling; either an unrecognized structurally higher normal fault or a Late Cretaceous pluton at depth, are permissive.

Motion along the Pinto shear zone is contemporaneous with other extensional structures, regional exhumation and cooling of mid-crustal rocks, in the eastern Mojave Desert. We contend that the common 74–68 Ma cooling ages in the Mojave Desert region may in many cases record post-intrusive cooling and exhumation by extensional structures. Refrigeration of the Cordilleran lithosphere (Dumitru et al., 1991) or erosional denudation (George and Dokka, 1994) may be locally important, and refrigeration should postdate cooling related to extension and erosion. Late Cretaceous extension at 75–68 Ma was regional in scale in the southwestern Cordillera, and therefore requires a regional causative mechanism. We propose that widespread Late Cretaceous crustal melting and magmatism followed by extension and cooling in the Mojave sector of the Cordilleran orogen is most consistent with production of a low-viscosity lower crust during anatexis and/or removal of

mantle lithosphere at the onset of Laramide shallow subduction. From the perspective of the Sevier and Laramide orogens as a composite contractional orogen, the extension and magmatism in the Mojave Desert region was synchronous with continued convergence between the Farallon and North America plates, and continued shortening in the Sevier fold–thrust belt and Laramide province to the north and in the Laramide province to the south.

Acknowledgements

References

Allmendinger, R.W., 2001. FaultKin v.4.1X, A program for analyzing fault slip data for Mac OSX.

Anderson, J.L., Barth, A.P., Young, E.D., Bender, E.E., Davis, M.J., Faber, D.L., Hayes, E.M., Johnson, K.A., 1992. Plutonism across the Tujunga–North American terrane boundary; a middle to upper crustal view of two juxtaposed magmatic arcs. In: Bartholomew, M.J., Hyndman, D.W., Mogk, D.V., Mason, R. (Eds.), Characterization and Composition of Ancient (Precambrian to Meszoic) Continental Margins Proceedings of the Eighth International Conference on Basement Tectonics, Holland 8, pp. 205–230.

Andrew, J.E., 2001. Insight into the arc tectonics of the southwestern Cordillera via the Mesozoic deformation history of the Panamint Range. Geological Society of America Abstracts with Programs 33, 208–209.

Annen, C., Sparks, R.S.J., 2002. Effects of repetitive emplacement of basaltic intrusions on thermal evolution and melt generation in the crust. Earth and Planetary Science Letters 203, 937–955.

Applegate, J.D., Hodges, K.V., 1995. Mesozoic and Cenozoic extension recorded by metamorphic rocks in the Funeral Mountains, California. Geological Society of America Bulletin 107, 1063–1076.

Applegate, J.D.R., Walker, J.D., Hodges, K.V., 1992. Late Cretaceous extensional unroofing in the Funeral Mountains metamorphic core complex, California. Geology 19, 519–522.

Armstrong, R.L., 1982. Cordilleran metamorphic core complexes—from Arizona to southern Canada. Annual Review of Earth and Planetary Science Letters 10, 129–154.

Armstrong, R.L., Suppe, J., 1973. Potassium–Argon geochronometry of Mesozoic igneous rocks in Nevada, Utah, and Southern California. Geological Society of America Bulletin 84, 1375–1391.

Bailey, C.M., Eyster, E.L., 2003. General shear deformation in the Pinaleño Mountains metamorphic core complex, Arizona. Journal of Structural Geology 25, 1883–1892.

Barth, A.P., Wooden, J.L., Jacobsen, C.E., Probst, K., 2004. U–Pb geochronology and geochemistry of the McCoy Mountains Formation, southeastern California: a Cretaceous retroarc foreland basin. Geological Society of America Bulletin 116, 142–163.

Barton, M.D., 1990. Cretaceous magmatism, metamorphism, and metallogeny in the east-central Great Basin. In: Anderson, J.L. (Ed.), The Nature and Origin of Cordilleran Magmatism Geological Society of America Memoir, 174, pp. 283–302.

Beckerman, G.M., Robinson, J.P., Anderson, J.L., 1982. The Teutonia batholith: a large intrusive complex of Jurassic and Cretaceous age in the eastern Mojave Desert, California. In: Frost, C.G., Martin, D.L. (Eds.), Mesozoic–Cenozoic Tectonic Evolution of the Colorado River, California, Arizona, and Nevada. Cordilleran Publishers, San Diego, CA, pp. 205–221.

Berth'e, D., Choukroune, P., Jegouzo, P., 1979. Orthogneiss, mylonite and non-coaxial deformation of granites: the example of the South American shear zone. Journal of Structural Geology 1, 31–42.

Beyene, M.A., 2000. Kinematics and timing of the Pinto Shear Zone, New York Mountains, Northeastern Mojave Desert, California. MS thesis, University of Nevada, Las Vegas.

Bird, P., 1979. Continental delamination and the Colorado Plateau. Journal of Geophysical Research 84, 7561–7571.

Bird, P., 1984. Laramide crustal thickening event in the Rocky Mountain foreland and Great Plains. Tectonics 3, 741–758.

Boettcher, S.S., Mosher, S., 1998. Mid- to Late-Cretaceous ductile deformation and thermal evolution of the crust in the northern Dome Rock mountains, Arizona. Journal of Structural Geology 20, 745–764.

Boullier, A.M., Bouchez, J.L., 1975. Le quartz en rubans dans les mylonites. Bulletin of the Geological Society of France 7, 253–262.

Burchfiel, B.C., Davis, G.A., 1971. Clark Mountain thrust complex in the Cordillera of southeastern California: geologic summary and field trip guide. In: Elders, W.A. (Ed.), Geological Excursions in Southern California. University of California, Riverside, pp. 1–28.

Burchfiel, B.C., Davis, G.A., 1976. Compression and crustal shortening in Andean-type orogenesis. Nature 260, 693–694.

Burchfiel, B.C., Davis, G.A., 1977. Geology of the Sagamore Canyon–Slaughterhouse Spring area, New York Mountains, California. Geological of America Bulletin 88, 1623–1640.

Burchfiel, B.C., Davis, G.A., 1981. Mojave Desert and environs. In: Ernst, W.G. (Ed.), The Geotectonic Development of California, Rubey Volume I. Prentice-Hall, Englewood Cliffs, NJ, pp. 217–252.

Burchfiel, B.C., Cowan, D.S., Davis, G.A., 1992. Tectonic overview of the Cordilleran orogen in the western United States. In: Burchfiel, B.C., Lipman, P.W., Zoback, M.L. (Eds.), The Cordilleran Orogen: Conterminous US. Geological Society of America, Boulder, CO, pp. 407–479.

Camilleri, P.A., Chamberlain, K.R., 1997. Mesozoic tectonics and metamorphism in the Pequop Mountains and Wood Hills region, northeast Nevada: implications for the architecture and evolution of the Sevier orogen. Geological Society of America Bulletin 109, 74–94.

Carl, B.C., Miller, C.F., Foster, D.A., 1991. Western Old Woman Mountains shear zone: evidence for latest Cretaceous core complex development in the southeastern California. Geology 19, 893–896.

Crittenden, M.-J., Coney, P.J., Davis, G.H. (Eds.), 1980. Cordilleran Metamorphic Core Complexes Geological Society of America Memoir 153.

Cross, T.A., Pilger, R.H., 1978. Tectonic controls of Late Cretaceous sedimentation, western interior USA. Nature 274, 653–657.

Decelles, P.G., Lawton, T.F., Mitra, G., 1995. Thrust timing, growth of structural culminations, and synorogenic sedimentation in the type Sevier orogenic belt, Western United States. Geology 23, 699–702.

Dewitt, E., Armstrong, R.L., Sutter, J.F., Zartman, R.E., 1984. U–Th–Pb, Rb–Sr, and Ar–Ar mineral and whole rock isotope systematics in a metamorphosed granitic terrane, southeastern California. Geological Society of America Bulletin 95, 723–739.

Dickinson, W.R., Klute, M.A., Michael, J., Janecke, S.U., Lundin, E.R., McKittrick, M.A., Olivares, M.D., 1988. Paleogeographic and

paleotectonic setting of Laramide sedimentary basins in the central Rocky Mountains region. Geological Society of America Bulletin 100, 1023–1039.

Dumitru, T.A., Gans, P.B., Foster, D.A., 1991. Refrigeration of the western Cordilleran lithosphere during Laramide shallow-angle subduction. Geology 19, 1145–1148.

Dunkl, I., Grasemann, B., Frisch, W., 1998. Thermal effects of exhumation of a metamorphic core complex on hanging wall syn-rift sediments: an example from the Rechnitz Window, Eastern Alps. Tectonophysics 297, 31–50.

Engebretson, D.C., Cox, A., Gordon, R.G., 1985. Relative motions between oceanic and continental plates in the Pacific basin. Geological Society of America Special Paper 206.

England, P.C., Houseman, G.A., 1988. The mechanics of the Tibetan Plateau. Philosophical Transactions of the Royal Society London A326, 301–319.

England, P.E., Thompson, A.B., 1984. Pressure–temperature–time paths of regional metamorphism, I, Heat transfer during the evolution of regions of thickened crust. Journal of Petrology 97, 894–928.

Everndon, J.F., Kistler, R.W., 1970. Chronology of emplacement of Mesozoic batholithic complexes in California and western Nevada. US Geological Survey Professional Paper, Report P0623.

Farmer, G.L., DePaolo, D.J., 1983. Origin of Mesozoic and Tertiary granite in the western United States and implications for pre-Mesozoic crustal structure: 1, Nd and Sr isotopic studies in the geocline of the northern Great Basin. Journal of Geophysical Research 88, 3379–3401.

FitzGerald, J.D., Stünitz, H., 1993. Deformation of granitoids at low metamorphic grade I: reactions and grain size reduction. Tectonophysics 221, 299–324.

Fleck, R.J., Mattinson, J.M., Busby, C.J., Carr, M.D., Davis, G.A., Burchfiel, B.C., 1994. Isotopic complexities and the age of the Delfonte volcanic rocks, eastern Mescal Range, southeastern California: stratigraphic and tectonic implications. Geological Society of America Bulletin 106, 1242–1253.

Fletcher, J.M., Karlstrom, K.E., 1990. Late Cretaceous ductile deformation, metamorphism, and plutonism in the Piute Mountains, eastern Mojave Desert. Journal of Geophysical Research 95, 487–500.

Foster, D.A., Hyndman, D.W., 1990. Magma mixing and mingling between synplutonic mafic dikes and granite in the Idaho–Bitterroot batholith. In: Anderson, J.L. (Ed.), The Nature and Origin of Cordilleran Magmatism Geological Society of America Memoir, 174, pp. 347–358.

Foster, D.A., John, B.E., 1999. Quantifying tectonic exhumation in an extensional orogen with thermochronology; examples from the southern Basin and Range Province. In: Ring, U., Brandon, M.T., Lister, G.S., Willett, S.D. (Eds.), Exhumation Processes, Normal Faulting, Ductile Flow and Erosion Geological Society of London, London, United Kingdom Special Publications 154, pp. 343–364.

Foster, D.A., Harrison, T.M., Miller, C.F., 1989. Age, inheritance, and uplift history of the Old Woman–Piute batholith, California, and implications for K-feldspar age spectra. Journal of Geology 97, 232–243.

Foster, D.A., Harrison, T.M., Miller, C.F., Howard, K.A., 1990. $^{40}Ar/^{39}Ar$ thermochronology of the eastern Mojave Desert, California, and adjacent western Arizona with implications for the evolution of metamorphic core complexes. Journal of Geophysical Research 95, 20005–20024.

Foster, D.A., Miller, C.F., Harrison, T.M., Hoisch, T.D., 1992. $^{40}Ar/^{39}Ar$ thermochronology and thermobarometry of metamorphism, plutonism, and tectonic denudation in the Old Woman Mountains area, California. Geological Society of America Bulletin 104, 176–191.

Fox, L.K., Miller, D.M., 1995. Jurassic granitoids and related rocks of the southern Bristol Mountains, southern Providence Mountains, and Colton Hills, Mojave Desert, California. In: Anderson, J.L. (Ed.), Geological Society of America Memoir 174, pp. 111–132.

George, P.G., Dokka, R.K., 1994. Major Late Cretaceous cooling events in the eastern Peninsular Ranges, California, and their implications for Cordilleran tectonics. Geological Society of America Bulletin 106, 903–914.

Gerber, M.E., Miller, C.F., Wooden, J.L., 1995. Plutonism at the eastern edge of the Cordilleran Jurassic magmatic belt, Mojave Desert, California. In: Miller, D.M., Busby, C. (Eds.), Geological Society of America Special Paper 299, pp. 351–374.

Glazner, A.F., Walker, J.D., Fletcher, J.M., Bartley, J.M., Schermer, E.R., Martin, M.W., Boettcher, S., Miller, J.S., Linn, J.K., Fillmore, R.P., 1994. Reconstruction of the Mojave Block. In: McGill, S.F., Ross, T.M. (Eds.), Geological Investigations of an Active Margin Geological Society of America Cordilleran Section Guidebook, pp. 3–30.

Grasemann, B., Mancktelow, N.S., 1993. Two-dimensional thermal modeling of normal faulting; the Simplon fault zone, Central Alps, Switzerland. Tectonophysics 225, 155–165.

Hamilton, W.B., 1987. Mesozoic geology and tectonics of the Big Maria Mountains region, southeastern California. Arizona Geological Society Digest 18, 33–47.

Harris, N., Massey, J., 1994. Decompression and anatexis of the Himalayan metapelites. Tectonics 13, 1537–1546.

Henderson, L.J., Gordon, R.G., Engebretsen, D.C., 1984. Mesozoic aseismic ridges on the Farallon plate and southward migration of shallow subduction during the Laramide orogeny. Tectonics 3 (2), 121–132.

Hirth, G., Tullis, J., 1992. Dislocation creep regimes in quartz aggregates. Journal of Structural Geology 14, 145–159.

Hodges, K.V., Walker, J.D., 1990. Thermobarometric constraints on the unroofing history of a metamorphic core complex, Funeral Mountains, SE California. Journal of Geophysical Research 95, 8437–8445.

Hodges, K.V., Walker, J.D., 1992. Extension in the Cretaceous Sevier orogen, North American Cordillera. Geological Society of American Bulletin 104, 560–569.

Hodges, K.V., McKenna, L.W., Harding, M.B., 1990. Structural unroofing of the central Panamint Mountains, Death Valley region, southeastern California. In: Wernicke, B.P. (Ed.), Basin and Range Extensional Tectonics near the Latitude of Las Vegas, Nevada Geological Society of America Memoir 176, pp. 377–390.

Hoisch, T.D., 1987. Heat transport by fluids during Late Cretaceous regional metamorphism in the Big Maria Mountains, southeastern California. Geological Society of America Bulletin 98, 549–553.

Hoisch, T.D., Hamilton, W.B., 1990. Granite generation by fluid-induced anatexis. Eos 71 (19), 694.

Hoisch, T.D., Simpson, C., 1993. Rise and tilt of metamorphic rocks in the lower plate of a detachment fault in the Funeral Mountains, Death Valley, California. Journal of Geophysical Research 98, 6805–6827.

Hoisch, T.D., Heizler, M.T., Zartman, R.E., 1997. Timing of detachment faulting in the Bullfrog Hills and Bare Mountain area, southwest Nevada: inferences from $^{40}Ar/^{39}Ar$, K–Ar, U–Pb, and fission track thermochronology. Journal of Geophysical Research 102, 2815–2833.

Horinga, E.D., 1988. Ductile deformation associated with the Scanlon thrust in the Kilbeck Hills, southeastern California. Geological Society of America Abstracts with Programs 20, 170.

Houseman, G.A., McKenzie, D.P., Molnar, P., 1981. Convective instability of a thickened boundary layer and its relevance for the thermal evolution of continental convergent belts. Journal of Geophysical Research 86, 6115–6132.

Howard, K.A., John, B.E., Miller, C.F., 1987. Metamorphic core complexes, Mesozoic ductile thrusts, and Cenozoic detachments: Old Woman Mountains–Chemehuevi Mountains transect, California and Arizona. In: Davis, G.A., VanderDolder, E.M. (Eds.), Geologic Diversity of Arizona and its Margins: Excursions to Choice Areas Arizona Bureau of Geology and Mineral Technology Special Paper 5, pp. 365–382.

Howard, K.A., McCaffrey, K.J.W., Wooden, J.L., Foster, D.A., Shaw, S.E., 1995. Jurassic thrusting of Precambrian basement over Paleozoic cover

in the Clipper Mountains, southeastern California. In: Miller, D.M., Busby, C. (Eds.), Geological Society of America Special Paper 299, pp. 375–392.

Isacks, B.L., 1988. Uplift of the central Andean plateau and bending of the Bolivian orocline. Journal of Geophysical Research 93, 3211–3231.

Jacobson, C.E., 1990. The ^{40}Ar/^{39}Ar geochronology of the Pelona Schist and related rocks, Southern California. Journal of Geophysical Research 95, 509–528.

Jacobson, C.E., Oyarzabal, F.R., Haxel, G.B., 1996. Subduction and exhumation of the Pelona–Orocopia–Rand schists, southern California. Geology 24, 547–550.

Jennings, C.W. (compiler), 1977. Geologic map of California. California Division of Mines and Geology, scale 1:750,000.

John, B.E., Mukusa, S.B., 1990. Footwall rocks to the mid-Tertiary Chemehuevi Detachment fault: a window into the middle crust in the southern Cordillera. Journal of Geophysical Research 95, 463–485.

Jordan, T., Isacks, B., Allmendinger, R., Brewer, J., Ramos, V., Ando, C., 1983. Andean tectonics related to the geometry of the subducted plate. Geological Society of America Bulletin 94, 341–361.

Kapp, J.D., Miller, C.F., Miller, J.S., 2002. Ireteba Pluton, Eldorado Mountains, Nevada: late, deep-source, peraluminous magmatism in the Cordilleran interior. Journal of Geology 110, 649–669.

Kay, S.M., Abbruzzi, J.M., 1996. Magmatic evidence for Neogene lithospheric evolution of the central Andean 'flat-slab' between 30°S and 32°S. Tectonophysics 259, 15–28.

Kay, R.W., Kay, S.M., 1993. Delamination and delamination magmatism. Tectonophysics 219, 177–189.

Ketcham, R.A., 1996. Thermal models of core-complex evolution in Arizona and New Guinea: implications for ancient cooling paths and present-day heat flow. Tectonics 15, 933–951.

Kirschner, D.L., Cosca, M.A., Masson, H., Hunziker, J.C., 1996. Staircase ^{40}Ar/^{39}Ar spectra of fine-grained white mica: timing and duration of deformation and empirical constraints on argon diffusion. Geology 24, 747–750.

Kistler, R.W., Peterman, Z.E., 1978. Reconstruction of crustal blocks of California on the basis of initial strontium isotopic compositions of Mesozoic granitic rocks. US Geological Survey Professional Paper 1071.

Kula, J.L., 2002. Thermochronology and geobarometry of the Granite Mountains, southeastern California: exhumation of a plutonic complex during collapse of the Sevier orogen. MS thesis, University of Nevada, Las Vegas.

Kula, J.L., Spell, T.L., Wells, M.L., 2002. Syntectonic intrusion and exhumation of a Mesozoic plutonic complex in the Late Cretaceous, Granite Mountains, southeastern California. Geological Society of America Abstracts with Programs 34, 249.

Law, R.D., Knipe, R.J., Dayan, H., 1984. Strain path partitioning within thrust sheets: microstructural and petrofabric evidence from the Moine thrust zone at Loch Eriboll, northwest Scotland. Journal of Structural Geology 6, 477–498.

Lee, J., Miller, E.L., Sutter, J.F., 1987. Ductile strain and metamorphism in an extensional tectonic setting—a case study from the northern Snake Range, Nevada, USA. In: Coward, M.P., Dewey, J.F., Hancock, P.L. (Eds.), Continental Extensional Tectonics Geological Society Special Publications 28, pp. 267–298.

Lee, C.-T., Yin, Q., Rudnick, R.L., Jacobsen, S.B., 2001. Preservation of ancient and fertile lithospheric mantle beneath the southwestern United States. Nature 411, 69–73.

Leventhal, J.A., Reid, M.R., Montana, A., Holden, P., 1995. Mesozoic invasion of crust by MORB-source asthenospheric magmas, US Cordilleran interior. Geology 23, 399–402.

Lister, G.S., Davis, G.A., 1989. The origin of metamorphic core complexes and detachment faults formed during Tertiary continental extension in the northern Colorado River region, USA. Journal of Structural Geology 11, 65–94.

Lister, G.S., Snoke, A., 1984. S–C mylonites. Journal of Structural Geology 6, 617–638.

Lovera, O.M., 1992. Computer programs to model ^{40}Ar/^{39}Ar diffusion data from multidomain samples. Computers & Geosciences 18, 789–813.

Lovera, O.M., Richter, F.M., Harrison, T.M., 1989. ^{40}Ar/^{39}Ar thermochronometry for slowly cooled samples having a distribution of diffusion domain sizes. Journal of Geophysical Research 17, 917–935.

Lovera, O.M., Richter, F.M., Harrison, T.M., 1991. Diffusion domains determined by ^{39}Ar released during step heating. Journal of Geophysical Research 96, 2057–2069.

Lovera, O.M., Grove, M., Harrison, T.M., Mahon, K.I., 1997. Systematic analysis of K-feldspar ^{40}Ar/^{39}Ar step-heating experiments I: significance of activation energy determinations. Geochimica et Cosmochimica Acta 61, 3171–3192.

Malin, P.E., Goodman, E.D., Henyey, T.L., Li, Y.G., Okaya, D.A., Saleeby, J.B., 1995. Significance of seismic reflections beneath a tilted exposure of deep continental crust, Tehachapi Mountains, California. Journal of Geophysical Research 100, 2069–2087.

Marrett, R.A., Allmendinger, R.W., 1990. Kinematic analysis of fault-slip data. Journal of Structural Geology 12, 973–986.

McDougall, I., Harrison, M.T., 1999. Geochronology and Thermochronology by the ^{40}Ar/^{39}Ar Method. Oxford University Press, New York. 269pp.

McGrew, A.J., 1993. The origin and evolution of the southern Snake Range decollement, east central Nevada. Tectonics 12, 21–34.

McKaffrey, K.J.W., Miller, C.F., Karlstrom, K.E., Simpson, C., 1999. Synmagmatic deformation patterns in the Old Woman Mountains, SE California. Journal of Structural Geology 21, 335–349.

Miller, C.F., 1985. Are strongly peraluminous magmas derived from mantle sedimentary (pelitic) sources? Journal of Geology 93, 673–689.

Miller, C.F., Barton, M.D., 1990. Phanerozoic plutonism in the Cordilleran interior, USA. In: Kay, M.S., Rapela, C.W. (Eds.), Plutonism from Antarctica to Alaska Geological Society of America Special Paper, 241, pp. 213–231.

Miller, C.F., Bradfish, L.J., 1980. An inner Cordilleran belt of muscovite-bearing plutons. Geology 8, 412–416.

Miller, D.M., Howard, K.A., 1985. Bedrock geologic map of the Iron Mountains Quadrangle, San Bernardino and Riverside counties, California. US Geological Survey, Report, MF-1736.

Miller, F.K., Morton, D.M., 1980. Potassium–argon geochronology of the eastern Transverse Ranges and southern Mojave Desert, southern California. US Geological Survey Professional Paper, Report, P1152, 30pp.

Miller, D.M., Wooden, J.L., 1993. Geologic map of the New York Mountains area, California and Nevada. US Geologic Survey Open-File Report 93-198, 10pp, scale 1:50,000.

Miller, D.M., Miller, R.J., Nielson, J.E., Wilshire, H.G., Howard, K.A., Stone, P., 1991. Preliminary geologic map of the East Mojave National Scenic Area, California. US Geological Survey Open-File Report 91-435, 8pp, scale 1:100,000.

Miller, D.M., Wells, M.L., Dewitt, E., Walker, J.D., Nakata, J.K., 1996. Late Cretaceous extensional fault system across the northeastern Mojave Desert. San Bernardino County Museum Association Quarterly 43 (1), 77–83.

Molnar, P., Lyon-Caen, H., 1988. Some simple physical aspects of the support, structure and evolution of mountain belts. In: Clark, S.P.-J. (Ed.), Processes in Continental and Lithospheric Deformation Geological Society of America Special Paper, 218, pp. 179–207.

Passchier, C.W., Simpson, C., 1986. Porphyroclast systems as kinematic indicators. Journal of Structural Geology 15, 895–910.

Passchier, C.W., Trouw, R.A., 1996. Microtectonics. Springer, Berlin, Germany. 289pp.

Patiño Douce, A.E., 1999. What do experiments tell us about the relative contributions of crust and mantle to the origin of granitic magmas? In: Castro, A., Fernandez, C., Vigneresse, J.L. (Eds.), Understanding granites: Integrating New and Classical Techniques Geological Society Special Publication 168, pp. 55–75.

Patiño Douce, A.E., Humphreys, E.D., Johnston, A.D., 1990. Anatexis and

metamorphism in tectonically thickened continental crust exemplified by the Sevier hinterland, western North America. Earth and Planetary Science Letters 97, 290–315.

Pease, V., Argent, J., 1999. The northern Sacramento Mountains, Southwest United States; Part I, structural profile through a crustal extensional detachment system. In: Mac Niocaill, C., Ryan, P.D. (Eds.), Continental Tectonics Geological Society Special Publications 164, pp. 179–198.

Platt, J.P., England, P.C., 1993. Convective removal of lithosphere beneath mountain belts: thermal and mechanical consequences. American Journal of Science 293, 307–336.

Pryer, L.L., 1993. Microstructures in feldspars from a major crustal thrust zone: the Grenville Front, Ontario, Canada. Journal of Structural Geology 15, 21–36.

Reynolds, S.J., Spencer, J.C., Richard, S.M., Laubach, S.E., 1986. Mesozoic structures in west-central Arizona. Arizona Geological Society Digest 16, 35–51.

Richter, F.M., Lovera, O.M., Harrison, T.M., Copeland, P., 1991. Tibetan tectonics from $^{40}Ar/^{39}Ar$ analysis of a single K-feldspar sample. Earth and Planetary Science Letters 105, 266–278.

Royden, L.H., 1993. Evolution of retreating subduction boundaries formed during continental collision. Tectonics 12, 629–638.

Ruppel, C., Hodges, K.V., 1994. Pressure–temperature–time paths from two-dimensional thermal models; prograde, retrograde, and inverted metamorphism. Tectonics 13, 17–44.

Ruppel, C., Royden, L., Hodges, K.V., 1988. Thermal modeling of extensional tectonics; application to pressure–temperature–time histories of metamorphic rocks. Tectonics 7, 947–957.

Sawyer, E.W., 1998. Formation and evolution of granitic magmas during crustal reworking: the significance of diatexites. Journal of Petrology 39, 1147–1167.

Schermer, E.R., Busby, C., 1994. Jurassic magmatism in the central Mojave Desert; implications for arc paleogeography and preservation of continental volcanic sequences. Geological Society of America Bulletin 106, 767–790.

Sheets, R.W., 1996. Geology and mineralization in the vicinity of the Morning Star precious-metal deposit of the Ivanpah Mountains, San Bernardino County, California. PhD Dissertation, VPI, Blacksburg, VA.

Simpson, C., DePaor, D.G., 1993. Strain and kinematic analysis in general shear zones. Journal of Structural Geology 15, 1–20.

Simpson, C., Wintsch, R.P., 1989. Evidence for deformation-induced K-feldspar replacement by myrmekite. Journal of Metamorphic Geology 7, 261–275.

Smith, A.G., Wells, M.L., Foster, D.A., 2003. Timing and development of an orogen-parallel lineation and of frontal thrusting in the southern Cordilleran fold–thrust belt, New York Mountains, California. Geological Society of America Abstracts with Programs, 25.

Stewart, S.A., Argent, J.D., 2000. Relationship between polarity of extensional fault arrays and presence of detachments. Journal of Structural Geology 22, 693–711.

Stipp, M., Stünitz, J., Heilbronner, R., Schmid, S.M., 2002. The eastern

Tonale fault zone: a 'natural laboratory' for crystal-plastic deformation of quartz over a temperature range of 250–700 °C. Journal of Structural Geology 24, 1861–1884.

Sutter, J.F., 1968. Chronology of major thrusts, southern Great Basin, California. MS Thesis, Rice University.

Vanderhaeghe, O., Teyssier, C., 2001. Partial melting and flow of orogens. Tectonophysics 342, 451–472.

Walker, J.D., Burchfiel, B.C., Davis, G.A., 1995. New age controls on initiation and timing of foreland belt thrusting in the Clark Mountains, Southern California. Geological Society of America Bulletin 107, 742–750.

Wallis, S.R., 1992. Vorticity analysis in metachert from the Sanbagawa Belt, SW Japan. Journal of Structural Geology 14, 271–280.

Wells, M.L., 2001. Rheological control on the initial geometry of the Raft River detachment fault and shear zone, western United States. Tectonics 20, 435–457.

Wells, M.L., Dallmeyer, R.D., Allmendinger, R.W., 1990. Late Cretaceous extension in the hinterland of the Sevier thrust belt, northwestern Utah and southern Idaho. Geology 18, 929–933.

Wells, M.L., Hoisch, T.D., Peters, M.P., Miller, D.M., Wolff, E.W., Hanson, L.W., 1998. The Mahogany Peaks Fault, a Late Cretaceous–Early Paleocene normal fault in the hinterland of the Sevier Orogen. Journal of Geology 106, 623–634.

Wells, M.L., Snee, L.W., Blythe, A.E., 2000. Dating of major normal fault systems using thermochronology: an example from the Raft River detachment, Basin and Range, western United States. Journal of Geophysical Research 105, 16303–16327.

Wells, M.L., Spell, T.L., Grove, M., 2002. Late Cretaceous intrusion and extensional exhumation of the Cadiz Valley batholith, Iron Mountains, southeastern California. Geological Society of America Abstracts with Programs 34, 178.

Wernicke, B.P., 1992. Cenozoic extensional tectonics of the US Cordillera. In: Burchfiel, B.C., Lipman, P.W., Zoback, M.L. (Eds.), The Cordilleran Orogen: Conterminous. US Geological Society of America, Boulder, CO, pp. 553–581.

Wood, D.J., Saleeby, J.B., 1997. Late Cretaceous–Paleocene extensional collapse and disaggregation of the southernmost Sierra Nevada batholith. International Geology Review 39, 973–1009.

Wright, L.A., Troxel, B.W., 1993. Geologic map of the central and northern Funeral Mountains and adjacent areas, Death Valley region, Southern California: Miscellaneous Investigations Series. US Geological Survey, Report. I-2305, scale 1:48,000.

Wright, J.E., Wooden, J.L., 1991. New Sr, Nd, and Pb isotopic data from plutons in the northern Great Basin; implications for crustal structure and granite petrogenesis in the hinterland of the Sevier thrust belt. Geology 19, 458–460.

Yin, A., Kelty, T.K., 1991. Development of normal faults during emplacement of a thrust sheet: an example from the Lewis allochthon, Glacier National Park, Montana. Journal of Structural Geology 13, 37–47.

Yonkee, W.A., DeCelles, P.G., Coogan, J., 1997. Kinematics and synorogenic sedimentation of the eastern frontal part of the Sevier orogenic wedge, northern Utah. Brigham Young University Geological Studies 42, 355–380.